NJC

ROYAL SOCIETY OF CHEMISTRY

PAPER

View Article Online
View Journal | View Issue

Cite this: *New J. Chem.*, 2021, 45, 11136

1,2,4-Triazolo[4,3-*c*]quinazolines: a bioisosterism-guided approach towards the development of novel PCAF inhibitors with potential anticancer activity†

Mohamed H. El-Shershaby,[a] Adel Ghiaty,[a] Ashraf H. Bayoumi,[a] Hany E. A. Ahmed,[ab] Mona S. El-Zoghbi,[c] Khaled El-Adl[de] and Hamada S. Abulkhair[*af]

Targeting PCAF with small inhibitor molecules has emerged as a potential therapeutic strategy for the treatment of cancer. Recently, L-45 was identified as a potent triazolophthalazine inhibitor of the PCAF bromodomain. Here, we report the bioisosteric modification of the triazolophthalazine ring system of L-45 to its bioisosteric triazoloquinazoline while maintaining other essential structural fragments for effective binding with the binding site of PCAF. Consequently, a set of sixteen triazoloquinazoline derivatives were designed, synthesized, and investigated for their anticancer activity against four human cancer cell lines. Five derivatives demonstrated comparable cytotoxic activity with that of doxorubicin as a reference anticancer drug. Among them, compound **23** showed the most potent activity with IC_{50} values of 6.12, 4.08, 7.17, and 6.42 μM against HePG2, MCF-7, PC3, and HCT-116, respectively. Also, compound **21** exhibited comparable cytotoxic effects with that of doxorubicin against the selected cancer cell lines with IC_{50} values in the range of 7.41–9.58 μM. Molecular docking and pharmacokinetic studies were additionally performed to rationalize the binding affinities of the newly designed triazoloquinazolines toward the active site of histone acetyltransferase PCAF and to evaluate the druggability of new compounds. The results of these studies suggested that PCAF binding could be the mechanism of action of these derivatives.

Received 10th February 2021,
Accepted 17th May 2021

DOI: 10.1039/d1nj00710f

rsc.li/njc

1. Introduction

Cancer is a diverse collection of diseases that involve uncontrolled cell growth and have the potential to invade all the body organs. Over the past few decades, more than 150 anticancer agents have been approved by the FDA. Nevertheless, the majority of these approved chemotherapeutics negatively affect the patients' life. Consequently, unmet efforts for finding new effective and more safe anticancer agents remain crucial to treat the global growing number of patients. The irregular acetylation of histone is one of the aberrant DNA mutations linked to carcinogenesis.[1,2] Therefore, histone acetyltransferases have emerged as chemotherapeutic targets for developing anticancer agents.[1,3] Also, the unusual expression of the bromodomain family of proteins has been associated with abnormal cell proliferation.[4,5] New avenues for developing anticancer chemotherapeutics have been emphasized by the proven potent cytotoxicity of selective bromodomain inhibitor molecules.[6] The histone acetyltransferase paralogue p300/CBP-associated factor (PCAF) is a member of subfamily I of the phylogenetic bromodomain tree.[7] Mis-regulation of the latter bromodomain has been shown to be linked with a number of human diseases including cancer[8–10] and inflammatory disorders.[5] Mis-regulation of PCAF signaling is a predisposing factor for over-expression in a variety of cancer cells including hepatocellular,[11] mammary gland,[12] colorectal,[10] and prostate carcinoma.[13]

Quinazolines are a group of nitrogenous heterocycles that have gained particular importance as they are embedded in the core structures of many FDA-approved anticancer agents[14] (Fig. 1). These include gefitinib (**1**; Iressa), vandetanib (**2**; Caprelsa), erlotinib (**3**; Tarceva), lapatinib (**4**; Tykreb), afatinib (**5**; Gilotrif), and dacomitinib (**6**; Vizimpro). While the investigation of the

[a] *Pharmaceutical Organic Chemistry Department, Faculty of Pharmacy, Al-Azhar University, Nasr City 11884, Cairo, Egypt. E-mail: hamadaorganic@azhar.edu.eg*
[b] *Pharmacognosy and Pharmaceutical Chemistry Department, Pharmacy College, Taibah University, Al-Madinah Al-Munawarah 41477, Saudi Arabia*
[c] *Pharmaceutical Chemistry Department, Faculty of Pharmacy, Menoufia University, Gamal Abd El-Nasir Street, Shebin El-Koum, Egypt*
[d] *Department of Medicinal Chemistry & Drug Design, Faculty of Pharmacy, Al-Azhar University, Cairo, Egypt*
[e] *Department of Pharmaceutical Chemistry, Faculty of Pharmacy, Heliopolis University for Sustainable Development, Cairo, Egypt*
[f] *Pharmaceutical Chemistry Department, Faculty of Pharmacy, Horus University – Egypt, International Coastal Road, 34518, New Damietta, Egypt*
† Electronic supplementary information (ESI) available. See DOI: 10.1039/d1nj00710f

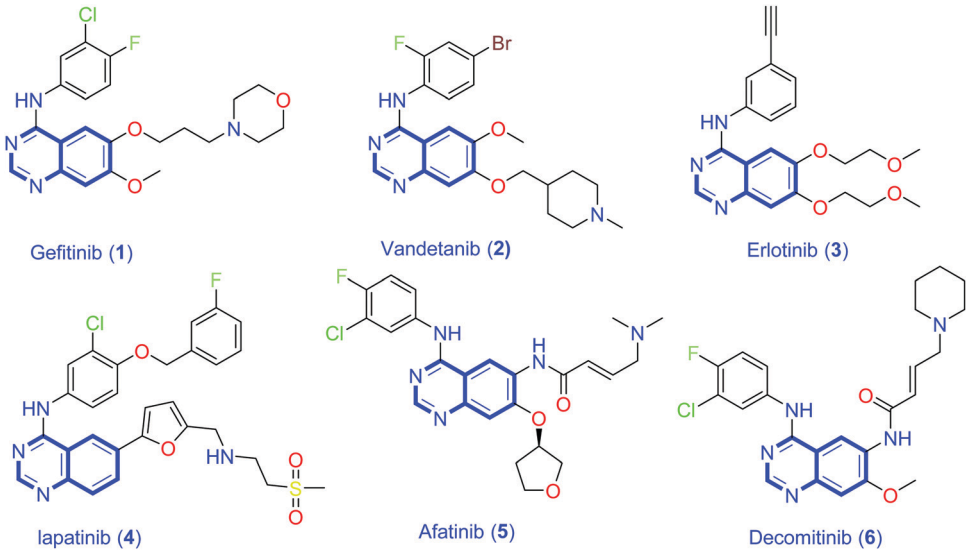

Fig. 1 Structures of quinazoline-derived FDA-approved anticancer agents.

anticancer activity of triazoloquinazoline derivatives has been described in a few articles,[15,16] both the quinazoline[17] and 1,2,4-triazole[18–20] derivatives have been individually recognized as anticancer drugs.

So far, six attempts have been accomplished for the development of triazoloquinazolines with antitumor activity.[21–26] Among these, two articles considered the annelation of a triazole ring to the quinazoline cycle to produce 1,2,4-triazolo[1,5-*c*]-quinazolines.[21,22] In the third one, a series of 1,2,4-triazolo[4,3-*a*]quinazolin-5-ones were designed as inhibitors of tubulin polymerization.[23] The results of the latter study revealed the potent anticancer activity of **7** and **8** against a panel of human cancer cell lines. Both compounds also presented potent inhibitory effects against tubulin polymerization. In 2014, the *in vitro* cytotoxicity evaluation of twenty two 1,2,4-triazolo[1,5-*a*]quinazolines revealed the higher cytotoxic effect of **9**, **10**, and **11** (Fig. 2) against medulloblastoma, hepatocellular carcinoma, and melanoma cell lines than dasatinib.[24] The last pair of articles was published in the previous year[25,26] and led to the detection of new 1,2,4-triazolo[4,3-*c*]quinazolines as a new class of DNA intercalators and potential inhibitors of topoisomerase II. These latter studies also reported the EGFR inhibition activity of **12**, **13**, and **14** (Fig. 2), with IC_{50} values in the range of 0.69–1.8 μM. Also, 1,2,4-triazolo[4,3-*c*]quinazoline derivative **15** (Fig. 2) was evaluated as a topoisomerase II inhibitor and DNA intercalator. The obtained results verified its inhibitory activity on topoisomerase II and the DNA binding affinity with IC_{50} values of 0.86 and 48.53 μM, respectively.

A few years ago, L-45 (**16**) was identified as the first potent, highly selective, and cell-active PCAF bromodomain inhibitor belonging to the class of 1,2,4-triazolo[3,4-*a*]phthalazines.[9] Our recent couple of research articles reported the design and PCAF bromodomain inhibitory effects of certain triazolopthalazines[18,27] as congeners of L-45. The PCAF antagonistic effect of L-45 was reported to be mediated through three key interactions with the binding site of histone acetyltransferase GCN5 (Fig. 3): (i) a π–π stacking interaction between the pyridazine ring and the Tyr1442 residue; (ii) a hydrogen bonding interaction between N-1 of the triazole ring and the Asn1436 residue; and (iii) an additional hydrogen bond between the side chain NH functionality attached to C-6 of the triazolophthalazine core and the Glu1389 residue. The aim of the present study is to develop new 1,2,4-triazolo-[4,3-*c*]quinazoline bioisosteric congeners of L-45 by fusion of the quinazoline and triazole ring as a suggested new scaffold of PCAF inhibitors with potent anticancer activity. This bioisosteric transformation is expected to furnish new derivatives capable of interacting with the PCAF receptor site in a similar pattern to that of L-45.

In medicinal chemistry, bioisosterism is a key concept that could be used for the modification of certain lead compounds to get safer and more clinically useful agents. Bioisosterism allows medicinal chemists to substitute constitutional fragments without significant perturbation in the biological activity. As initially specified by Friedman, bioisosteres must include all atoms and molecules which fit the widest definition for isosteres and have a similar type of biological activity.[28] A more recent definition of bioisosteres has been broadened to include compounds or groups that retain nearly equal molecular shapes and volumes, and approximately the same distribution of electrons, which exhibit similar physicochemical properties. The crucial component for bioisosterism is that bioisosteres are expected to affect the same biological target without considerable perturbation in the biological activity.[29] Overall, this strategy is an excellent tool for the optimization of lead compounds to obtain the desired potency and selectivity, and improved ADMET profiles for a marketable drug.[30] The *in silico* bioisosteric replacement mining approaches are divided into two types, ligand-based and structure-based. The former category uses information on ligands, whereas the latter requires knowledge of the biological target, as well as a specific understanding of the interactions between the ligand and target in the binding pocket.[31]

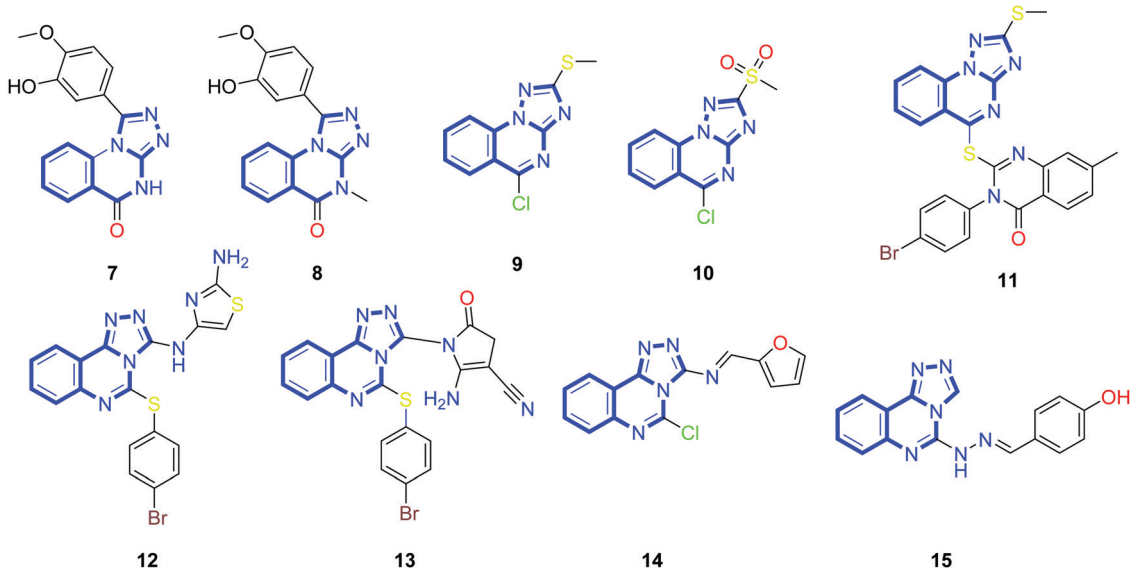

Fig. 2 Structures of selected [1,2,4]triazoloquinazines with potent anticancer activity.

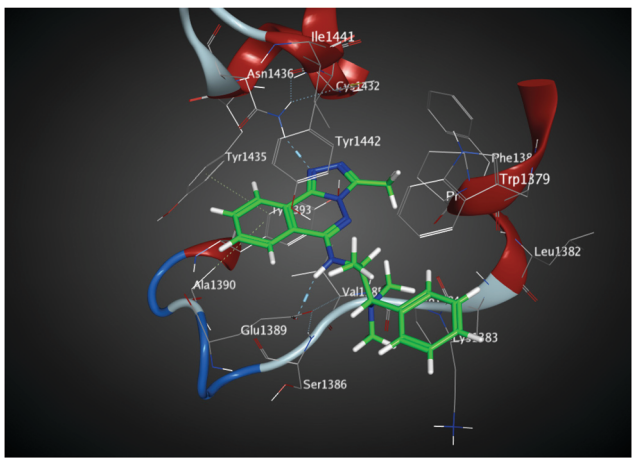

Fig. 3 The key interactions of L-45 with the active site of histone acetyltransferase GCN5.

1.1. Rationale and aim of the work

Considering the aforementioned facts, inspired by the versatilities of both the quinazoline and 1,2,4-triazole rings mentioned above, and as a continuation of our recent studies[32–35] on identifying new anticancer agents, synthesis of a new set of 1,2,4-triazolo-[4,3-*c*]quinazolines as L-45 bioisosteres was carried out to get new molecules with good potency. In the design of the new compounds, we employed the ligand-based bioisosterism strategy. Following the directions of bioisosterism, a number of constitutional fragments in the structure of lead compound L-45 and FDA approved anticancer quinazolines are expected to be substituted without significant perturbation in the activity. Accordingly, we considered keeping N-1 of the triazole ring in L-45 as an essential fragment that maintains the interaction with the essential amino acid residue Asn1436. However, three bioisosteric modifications were adopted in the newly designed derivatives (Fig. 4) to examine the effect of these structural optimizations on the anticancer and PCAF inhibitory potentials: First, the pyrimidine ring replaced the pyridazine ring of L-45 to keep the favorable π–π stacking interaction with the Tyr1442 residue. Second, diverse substitution patterns were introduced to position 5 of triazoloquinazoline scaffolds to investigate the effect on the cytotoxic activity. Last, the methyl group at C-3 of L-45 was replaced by three different substituent groups of different electronic and spatial characteristics. With this set of structural modifications, we decided to determine the significance of the HBD/HBA groups at C-6 of L-45 and the new compounds. All the new compounds were evaluated for their *in vitro* anticancer activity against four cancer cell lines, namely, hepatocellular carcinoma (HePG-2), mammary gland breast cancer (MCF-7), human prostate cancer (PC3), and colorectal carcinoma (HCT-116). In addition, the possible underlying mechanisms of these compounds were investigated *in silico* to rationalize their ability to bind with the active site of histone acetyltransferase GCN5 as a proposed mode of their anticancer activity. Also, the structure–activity relationship of the synthesized compounds was illustrated based on the results of cytotoxicity evaluation against four human cancer cell lines (HePG2, MCF-7, PC3, and HCT-116). Finally, ADMET profiles of the best effective derivatives were evaluated to determine their potential to build up as good drug candidates.

2. Results and discussion

2.1. Chemistry

The synthetic approach adopted for the synthesis of the starting 3-substituted-[1,2,4]triazolo[4,3-*c*]quinazolin-5(6*H*)-ones (**21–23**) is presented in Scheme 1. Briefly, a solution of potassium cyanate was added drop-wise into a solution of anthranilic acid in glacial acetic acid. The produced quinazoline-2,4(1*H*,3*H*)-dione was

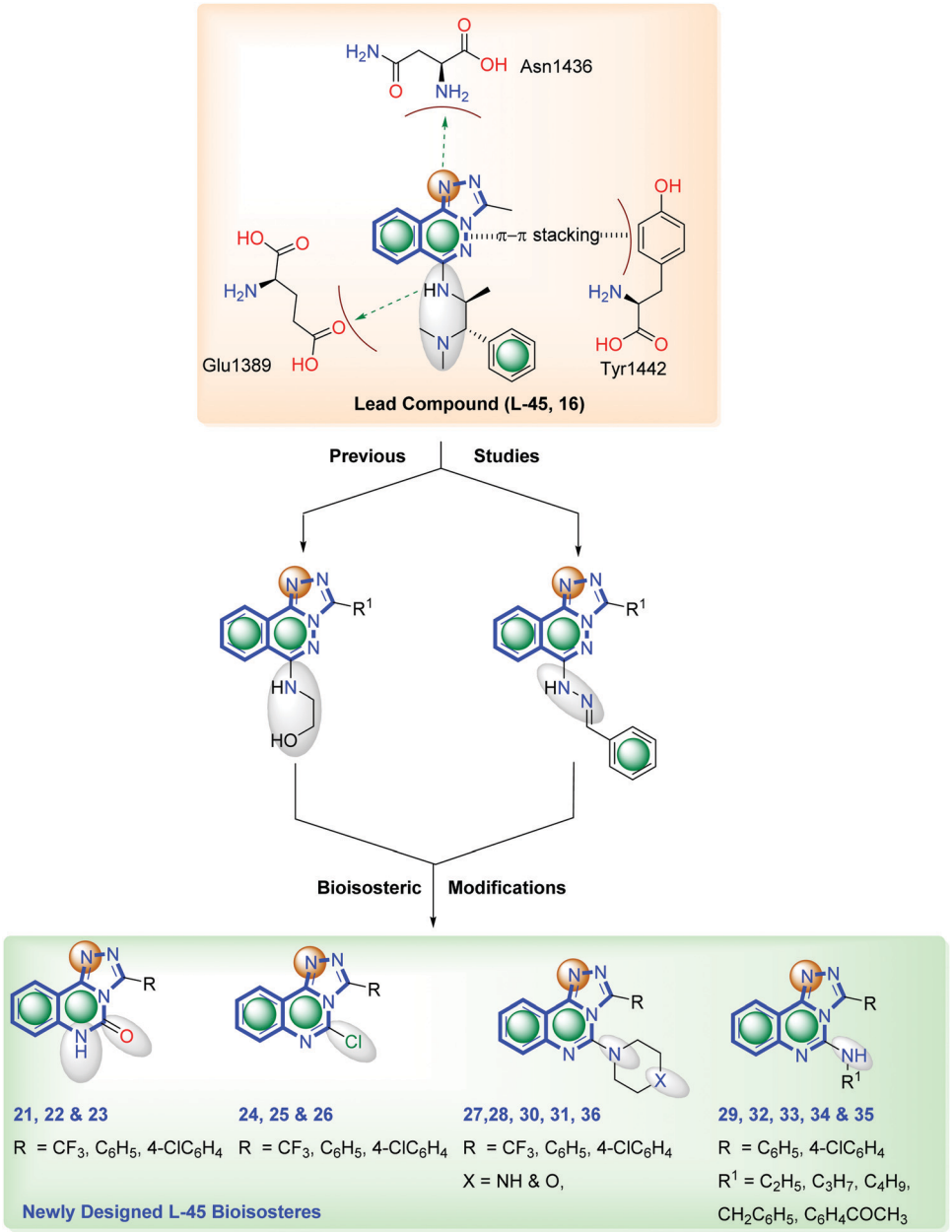

Fig. 4 Rational design of new suggested PCAF inhibitors.

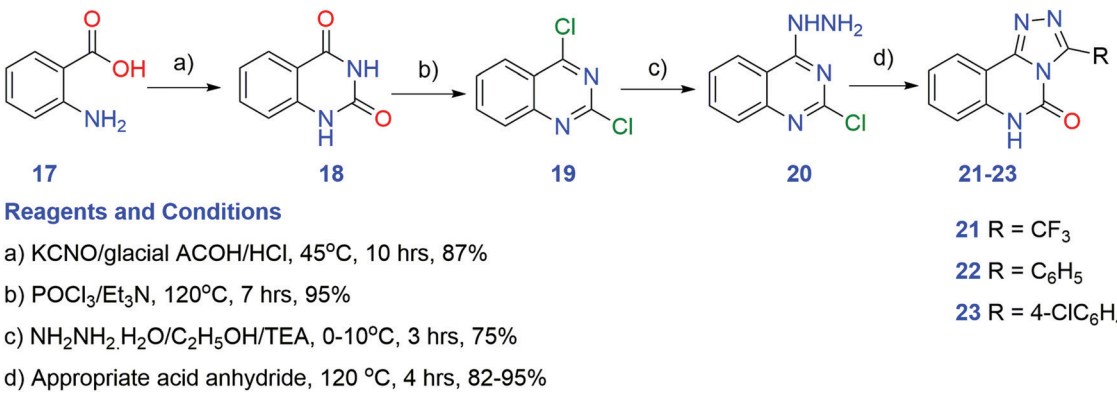

Scheme 1 Synthetic protocol of the starting triazoloquinazolines.

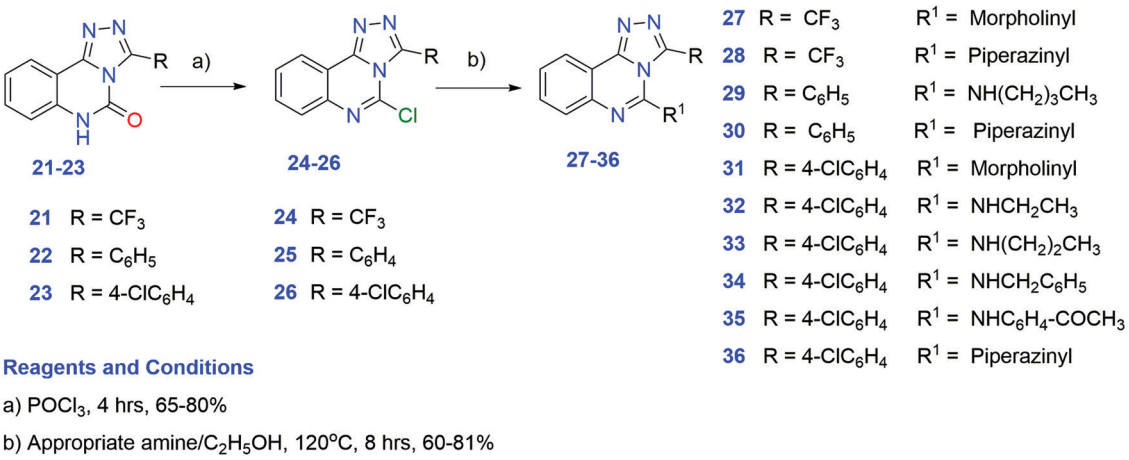

Scheme 2 Synthetic route of new triazoloquinazoline derivatives **24–36**.

treated with phosphorus oxychloride to get 2,4-dichloroquinazoline (**19**). The addition of hydrazine hydrate dropwise to the latter at 0–5 °C gives 2-chloro-4-hydrazinylquinazoline,[36,37] which was finally reacted with the appropriate acid anhydride[38] to obtain the desired starting 3-substituted-[1,2,4]triazolo[4,3-*c*]-quinazolin-5(6*H*)-one (**21–23**).

The structures of **21–23** were established based on their elemental and spectral data. The disappearance of the biforked absorption band of NH_2 of the starting hydrazinyl derivative together with the appearance of a new amidic C=O absorption band in the range of 1674–1697 cm^{-1} in the IR spectra confirmed the construction of the tricyclic ring. Also, the amidic NH revealed a singlet signal in the δ value range of 11.20–11.40 ppm which is D_2O exchangeable.

As presented in Scheme 2, our convergent synthesis approach of final target molecules **24–36** started by using a simple and straightforward strategy. Construction of this set of compounds was performed by converting the appropriate 3-substituted-[1,2,4]triazolo[4,3-*c*]quinazolin-5(6*H*)-one to its 5-chloro-3-substituted-[1,2,4]triazolo[4,3-*c*]quinazoline derivative by the action of phosphorus oxychloride. Treating these latter with different amine derivatives yielded our target compounds in reasonable yields and acceptable purities.[39–41] The selected approach depended on the highly reliable and well-established nucleophilic substitution reaction, exploiting the good commercial availability of amine derivatives. Adopting this approach, a set of ten triazoloquinazoline derivatives carrying an amine fragment at position 5 were afforded in yields ranging from 73 to 86%. All the IR, ^{1}H NMR, and ^{13}C NMR spectra of these derivatives were in accordance with the assumed structures. A piece of supporting evidence for the given produced structures was provided by element analysis and spectral data (see the ESI†). The ^{1}H nuclear magnetic resonance (NMR) spectrum of compound **27** as a representative example showed a triplet signal of four protons at 3.66 ppm equivalent to two methylene protons (CH_2) at positions 3 and 5 of the morpholinyl fragment. The ^{1}H NMR spectrum of the same compound revealed another triplet signal of another four protons at 3.60 ppm due to the two methylene protons at positions 2 and 6 of the morpholinyl side chain. ^{13}C NMR of **31** as a representative spectrum showed fifteen signals equivalent to fifteen carbon types, among them two in the aliphatic region at 67.00 and 45.89 ppm due to (CH_2OCH_2) and (CH_2NCH_2), respectively. The purity of the synthesized compounds was monitored by TLC and confirmed by elemental analysis.

2.2. Evaluation of the biological activity

2.2.1. Cytotoxicity assay. Four cancer cell lines were selected to evaluate the cytotoxic effects of the new compounds using the MTT colorimetric assay.[42] These cells include hepatocellular, mammary gland, colorectal, and prostate carcinoma. The selection of such cancer cells depended on the over-expression of PCAF in these cell types.[10–13] The cytotoxicity of the new 1,2,4-triazolo-[4,3-*c*]quinazoline bioisosteres of L-45 was compared with that of doxorubicin as a reference anticancer agent. Results of the preliminary antiproliferative evaluation are shown in Table 1. The tabulated results showed very strong to moderate cytotoxicity for six of the tested compounds against the selected four cancer cell lines. The concentrations of new ligands **21–26** necessary for 50% inhibition of tumor cell proliferation were found to be within the range of 4.08–24.50 μM. The compounds belonging to the [1,2,4]triazolo[4,3-*c*]quinazolin-5(6*H*)-one derivatives (**21–23**) and 5-chloro-[1,2,4]triazolo[4,3-*c*]quinazoline derivatives (**24–26**) with no substituent group at C-5 revealed better activity than those incorporating an *N*-alkyl/aralkyl amine substituent group at the same position. In regard to the tested cancer cells, the breast cancer cells (MCF-7) and colorectal cancer cells (HCT-116) were found to be the most sensitive to the cytotoxic effect of the new compounds followed by the prostate cancer cells (PC3). The hepatocarcinoma cells (HePG2) were found to be the least sensitive to the cytotoxic effect of our target compounds as indicated by the higher IC_{50} values presented.

2.3. Structure–activity relationship study

As outlined in the rational ligand-based drug design, studying the SAR of the newly designed 1,2,4-triazolo[4,3-*c*]quinazoline bioisosteres of L-45 as cytotoxic agents is a major objective of this work. Doxorubicin was selected as a reference anticancer drug to compare the cytotoxicity of the newly designed compounds as it

Table 1 *In vitro* anticancer activity of the designed new triazoloquinazolines[a]

			In vitro cytotoxicity IC_{50}[b] (μM)			
	R	R^1	HePG2	MCF-7	PC3	HCT-116
			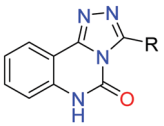			
DOX[c]	—	—	4.50 ± 0.2	4.17 ± 0.2	8.87 ± 0.6	5.23 ± 0.3
21	CF_3	—	7.41 ± 0.5	5.93 ± 0.4	9.58 ± 0.8	8.16 ± 0.7
22	C_6H_5	—	13.89 ± 1.1	16.21 ± 1.3	22.48 ± 1.8	12.08 ± 1.1
23	4-ClC_6H_4	—	6.12 ± 0.5	4.08 ± 0.5	7.17 ± 0.9	6.42 ± 0.7
			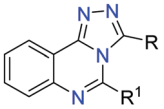			
24	CF_3	Cl	18.58 ± 1.5	19.57 ± 1.7	24.50 ± 2.0	13.28 ± 1.2
25	C_6H_5	Cl	11.26 ± 1.0	7.84 ± 0.7	14.09 ± 1.3	9.27 ± 0.8
26	4-ClC_6H_4	Cl	7.32 ± 0.8	5.38 ± 0.6	8.28 ± 0.8	8.15 ± 0.7
27	CF_3	Morpholin-4-yl	68.27 ± 3.8	80.54 ± 4.4	92.68 ± 4.9	47.19 ± 3.6
28	CF_3	Piperazin-1-yl	23.69 ± 1.9	21.04 ± 1.9	28.36 ± 2.2	15.49 ± 1.4
29	C_6H_5	$NH(CH_2)_3CH_3$	9.02 ± 0.8	6.38 ± 0.6	10.27 ± 1.0	8.56 ± 0.7
30	C_6H_5	Piperazin-1-yl	26.87 ± 2.3	15.81 ± 1.3	24.96 ± 2.1	9.38 ± 0.8
31	4-ClC_6H_4	Morpholin-4-yl	42.71 ± 2.9	58.39 ± 3.2	60.61 ± 3.5	31.97 ± 2.7
32	4-ClC_6H_4	$NHCH_2CH_3$	84.19 ± 4.5	93.48 ± 5.3	>100	61.45 ± 4.1
33	4-ClC_6H_4	$NH(CH_2)_2CH_3$	>100	>100	>100	67.69 ± 4.2
34	4-ClC_6H_4	$NHCH_2C_6H_5$	>100	>100	>100	88.16 ± 4.8
35	4-ClC_6H_4	NHC_6H_4-$COCH_3$	>100	>100	>100	>100
36	4-ClC_6H_4	Piperazin-1-yl	40.38 ± 2.8	58.16 ± 3.4	63.82 ± 3.5	39.17 ± 3.1

[a] Cancer cells were treated with the test compound for 72 h and the cytotoxicity is expressed as the concentration needed to inhibit 50% of tumor cell proliferation (IC_{50}). Data here are presented as the means of three independent experiments ± SD. [b] IC_{50} (μM): 1–10 (very strong), 11–20 (strong), 21–50 (moderate), 51–100 (weak) and above 100 (non-cytotoxic). [c] DOX: doxorubicin.

is a potent cytotoxic agent typically used in the treatment of a variety of carcinomas including hepatocellular carcinoma, breast, prostate, and colorectal cancers.[43,44] Based on the obtained results for the tested compounds and doxorubicin as a reference drug, the SAR of the anticancer activity of the synthesized compounds revealed a number of common findings. Except for the *N*-butylamine derivative **29**, there is a dramatic fall in the activity upon attachment of *N*-alkyl/aralkyl amine fragments at C-5 of the 1,2,4-triazolo[4,3-*c*]quinazoline ring system. This is noticeable upon comparing the *in vitro* cytotoxic activity of the [1,2,4]triazolo[4,3-*c*]-quinazolin-5(6*H*)-one derivatives (**21–23**) and 5-chloro-[1,2,4]-triazolo[4,3-*c*]quinazoline derivatives (**24–26**) with no substituent group with that of compounds **27**, **28**, and **30–36** incorporating an *N*-alkyl/aralkyl amine substituent group at the same position. This finding may indicate the importance of the presence of the HBD/HBA group at this position to enable the ligand to bind with the essential amino acid Glu1389 at the target protein binding site.[9] In this context, compounds **21** and **23** presented comparable cytotoxic effects with that revealed by the reference drug doxorubicin against all the tested cancer cells. In particular, compound **21** was the most potent derivative with IC_{50} values of 7.41, 5.93, 9.58, and 8.16 μM compared with 4.50, 4.17, 8.87, and 5.23 μM, respectively, of the reference cytotoxic agent against HePG2, MCF-7, PC3, and HCT-116, respectively. These results indicate the approximately equipotent activity of **21** and doxorubicin on breast and prostate cancer cells. Also, the 1,2,4-triazolo[4,3-*c*]quinazoline-triazolo[4,3-*c*]-quinazolin-5(6*H*)-one derivative with a 4-chlorophenyl substituent at C-3 (**23**) presented very strong cytotoxic effects with IC_{50} values of 6.12, 4.08, 7.17, and 6.42 μM against the HePG2, MCF-7, PC3, and HCT-116 cancer cell lines, respectively, compared with 4.50, 4.17, 8.87, and 5.23 μM, respectively, of doxorubicin. These findings indicate the approximately equipotent activity of **23** and doxorubicin on breast and colorectal cancer cells and even a better activity of **23** against the prostate cancer.

On the other hand, the nature of the substituents attached to C-3 of the triazole ring had no remarkable impact on the cytotoxicity. Accordingly, the compounds with substituents with a $-I$ effect, like CF_3, and substituents with a $+M$ effect, like C_6H_5 and 4-ClC_6H_4, at this position displayed comparable cytotoxic effects regardless of the nature of the C-3 attached group. Similarly, among the C-5 attached amine fragments, none of them had a positive effect on the anticancer potency. Individually, butylamine derivative **29** revealed good cytotoxic effects against the selected four cancer cells. Exceptionally, butylamine derivative **29** is approximately more than three-fold more potent (IC_{50} = 6.38–10.27 μM) against the tested cancer cells than the corresponding *N*-alkyl/aralkyl amine derivatives (**27**, **28** and **30–36**), which had moderate to weak cytotoxicity with IC_{50} values ≥15.49 μM. As well, the piperazinyl derivatives **28** and **30** were found to show moderate activity (IC_{50} = 9.38–28.36 μM). Among the *N*-alkyl/aralkyl derivatives, the *para*-acetylphenylamino derivative (**35**) revealed the least activity as an anticancer agent. This lower cytotoxic effect of such a compound may be attributed to the inability of such compounds to accommodate the target

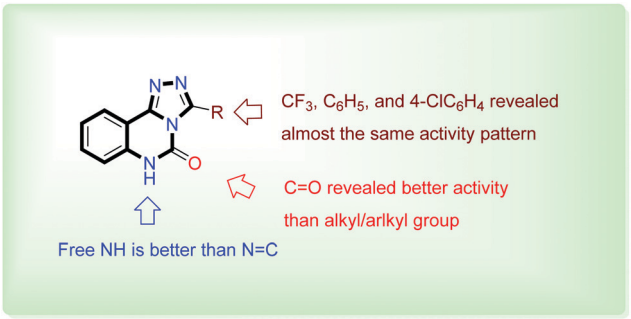

Fig. 5 Summary of the SAR study of the designed 1,2,4-triazolo[4,3-*c*]quinazolines.

protein binding site. These observations may collectively reflect the importance of the presence of a hydrogen bond donor group at position number six which is essential for binding with the Glu1389 fragment in the PCAF binding site.

In the analysis of each individual cancer cell, MCF-7 was shown to be potently inhibited by compounds **21**, **23**, **25**, and **26**, with IC_{50} values of 5.93, 4.08, 7.84, and 5.38 μM, respectively, compared with the reference drug (doxorubicin IC_{50} = 4.17 μM). Whereas, compounds **21**, **23**, and **26** effectively inhibited HePG2, with IC_{50} values of 7.41, 6.12, and 7.32 μM, respectively, compared with the reference drug (doxorubicin IC_{50} = 450 μM). The PC3 cell line was highly susceptible to the cytotoxic effect of compounds **21**, **23**, and **26** with IC_{50} values of 9.58, 7.17, and 8.28 μM, respectively, compared with the reference drug (doxorubicin IC_{50} = 8.87 μM). Similarly, the HCT-116 cell line was also significantly inhibited by the same latter three compounds with IC_{50} values of 8.16, 6.42, and 8.15 μM, respectively, compared with the reference drug (doxorubicin IC_{50} = 5.23 μM).

A diagrammatic description of the SAR of the antitumor activity for the synthesized L-54 bioisosteres is presented in Fig. 5.

2.4. Molecular docking study

A molecular docking study was performed to give guidance on the molecular binding modes of the target compounds inside the pocket of histone acetyltransferase. Docking was conducted using MOE2014 to determine the free energy and binding mode. The selection of promising molecules depends on both the perfect binding mode and the best binding free energy. The docking studies were validated in terms of the root mean square deviation (RMSD). Only poses possessing RMSD values within the acceptable range (0–1.20 Å) were considered.[45] With three main key interactions, the binding mode of L-45 in the active site of histone acetyltransferase GCN5 exhibited a binding energy of −11.52 kcal mol^{-1}. These interactions include π–π stacking between Tyr1442 and the pyridazine ring of L-45. As well, there is a hydrogen bond between the triazole ring and Asn1436 residue. The last interaction is presented in the form of another hydrogen bond between Glu1389 residues and the dimethylamino motif of L-45. An outline of the energy of binding, H-bonding interactions, and hydrophobic interactions of the newly designed L-45 bioisosteres and those of the re-docked internal co-crystallized ligand is shown in Table 2.

Table 2 Results of *in silico* docking scores for the new compounds and the co-crystallized ligand (L-45) with the binding site of histone acetyltransferase GCN5

			H-bonding interactions		Hydrophobic interactions	
Comp.	ΔG (kcal mol^{-1})	RMSD (Å)	Residue	Distance (Å)	Residue	Distance (Å)
L-45	−11.52	0.81	GLU 1389	3.47		
			GLU 1389	2.82		
			ASN 1436	3.40		
					TYR 1442	3.63
21	−10.15	0.98	ASN 1436	3.31		
					TYR 1442	3.62
22	−10.12	1.19			TRP 1379	4.10
					TRP 1379	4.34
					VAL 1385	3.60
					TYR 1442	3.77
23	−10.98	1.00	GLU 1389	3.09		
			THR 1401	3.24		
			ASN 1436	2.84		
					TYR 1442	3.85
					TYR 1442	3.84
24	−10.26	1.20	PRO 1380	3.20		
			ASN 1436	2.98		
					ALA 1390	4.52
					TYR 1442	3.65
25	−10.10	0.73	ASN 1436	2.99		
					TYR 1442	3.94
					TYR 1442	3.90
26	−10.74	1.11	THR 1401	3.42		
			ASN 1436	2.84		
					TYR 1442	3.90
					TYR 1442	3.80
27	−10.07	0.92	ASN 1436	3.45		
					TYR 1442	3.84
					TYR 1442	3.78
28	−9.79	0.80	CYS 1432	3.76		
			ASN 1436	2.71		
29	−11.556	1.162	ASN 1436	3.11		
					TYR 1442	3.98
30	−10.02	1.20			TYR 1442	3.74
					TRP 1379	4.15
31	−9.53	1.06	ASN 1436	2.93		
					TYR 1442	3.76
					TYR 1442	3.75
32	−9.55	0.89	THR 1401	3.44		
			ASN 1436	2.85		
					TYR 1442	3.91
					TYR 1442	3.79
33	−10.80	0.99	ASN 1436	2.85		
					TYR 1442	3.96
					TYR 1442	3.75
34	−9.78	1.16	THR 1401	3.42		
			ASN 1436	2.87		
					TYR 1442	3.95
					TYR 1442	3.75
35	−9.89	1.10	GLU 1389	2.97		
36	−9.92	1.19			TYR 1442	3.93

In all the newly designed L-45 bioisosteres, the pyrimidine rings revealed the same π–π stacking interaction with the essential amino acid residue Tyr1442. Also, *N*-1 of the triazole ring in the majority of the designed compounds formed a hydrogen bond with the second essential amino acid Asn1436 which is comparable with that formed by the co-crystallized ligand.

Unfortunately, the third interaction revealed by the co-crystallized ligand with the target protein active site is missing for almost all the new ligands. This finding may indicate the importance of the presence of a hydrogen bond donor fragment at position six whether in the triazolophthalazine or the triazoloquinazoline ring system. Individually, **23** revealed a standard interaction pattern and exhibited the best value of the binding free energy. The same compound exerted two additional favorable interactions in the form of π–π stacking and a hydrogen bond between the triazole ring and the chlorine atom of **23** and Tyr1442 and Thr1401, respectively. In particular, the binding modes of triazoloquinazolinones **21**, **22**, and **23** presented two essential binding interactions that are similar to those of L-45 with the active site of the target protein. Also, the distances of the hydrogen bonds and π–π contacts are comparable for the new triazoloquinazoline bioisosteres and the co-crystallized ligand. The pyrimidine rings of **21** and **23** showed π–π stacking interactions with Tyr1442 while *N*-1 formed hydrogen bonds with Asn1436. The phenyl side chain of **22** interacted with the protein binding site *via* π–π stacking interactions with Tyr1442 and an arene-H interaction with Glu1389. Two more favorable interactions were also observed as a bidirectional arene-H interaction between Trp1379 and the quinazoline ring of **22**. In regards to the 5-chloro-3-(substituted)-[1,2,4]triazolo[4,3-*c*]quinazoline derivatives **24–26**, they also presented the first two essential interactions of L-45 with Tyr1442 and Asn1436 with one or more additional favorable contacts. These include hydrogen bond and arene–H interactions between the chlorine atom and benzene ring of **24** and the Pro1380 and Ala1390 amino acid residues, respectively. The π–π stackings of **25** and **26** with Tyr1442 were found to be bidirectional to include both the triazole and pyrimidine rings of the triazoloquinazoline scaffold. The chlorine atom attached to the terminal phenyl ring of the **26** bioisostere of L-45 formed a hydrogen bond with the amino acid residue Thr1401. These additional desirable interactions and the relatively elevated binding free energy values (−10.10 to −10.98 kcal mol^{-1}) for the 1,2,4-triazolo[4,3-*c*]quinazolin-5(6*H*)-one and 5-chloro-3-(substituted)-[1,2,4]triazolo[4,3-*c*]quinazoline derivatives **21–26** may justify the superior *in vitro* anticancer activity of these derivatives. With almost much lower binding free energies, the other derivatives (**27–34**) showed binding modes which are also similar to those presented by the 1,2,4-triazolo[4,3-*c*]quinazolin-5(6*H*)-one and 5-chloro-3-(substituted)-[1,2,4]triazolo[4,3-*c*]quinazoline derivatives. Independently, *N*-butyl derivative **29** exhibited an affinity value of −11.55 kcal mol^{-1} and obeyed the same binding pattern with the binding site of histone acetyltransferase GCN5.

Collectively, the obtained results of the molecular docking studies showed that all the designed triazoloquinazoline bioisosteres of L-45 have almost similar positions and orientations inside the binding site of histone acetyltransferase GCN5. As well, the distribution of binding free energies calculated from the MOE software showed preferentially that the most active derivatives are highly correlated with the biological activity. Moreover, the absence of a hydrogen bond donor group at position 6 of the triazoloquinazoline ring system prohibited the formation of a hydrogen bond between the designed compounds and the Glu1389 amino acid residue. This missing interaction may explain the lower activities of the compounds with a substituent amine attached to C-5 of the triazoloquinazoline ring system. The 2-D and 3-D interaction patterns of the co-crystallized ligand L-45 and compounds with the best *in vitro* anticancer activity with the active site of histone acetyltransferase PfGCN5 (homologous Brd with PCAF) are presented in Fig. 6 and 7.

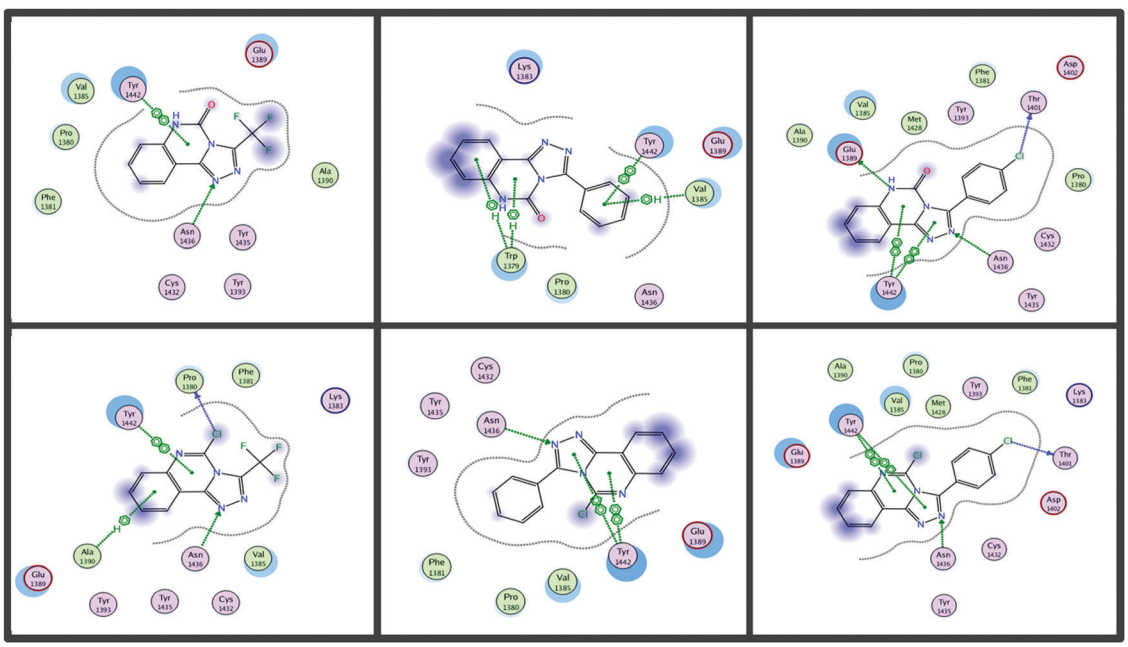

Fig. 6 3D binding interactions of **21** (upper left), **22** (upper middle), **23** (upper right), **24** (lower left), **25** (lower middle), and **26** (lower right) with the active site of histone acetyltransferase PfGCN5 (homologous Brd with PCAF).

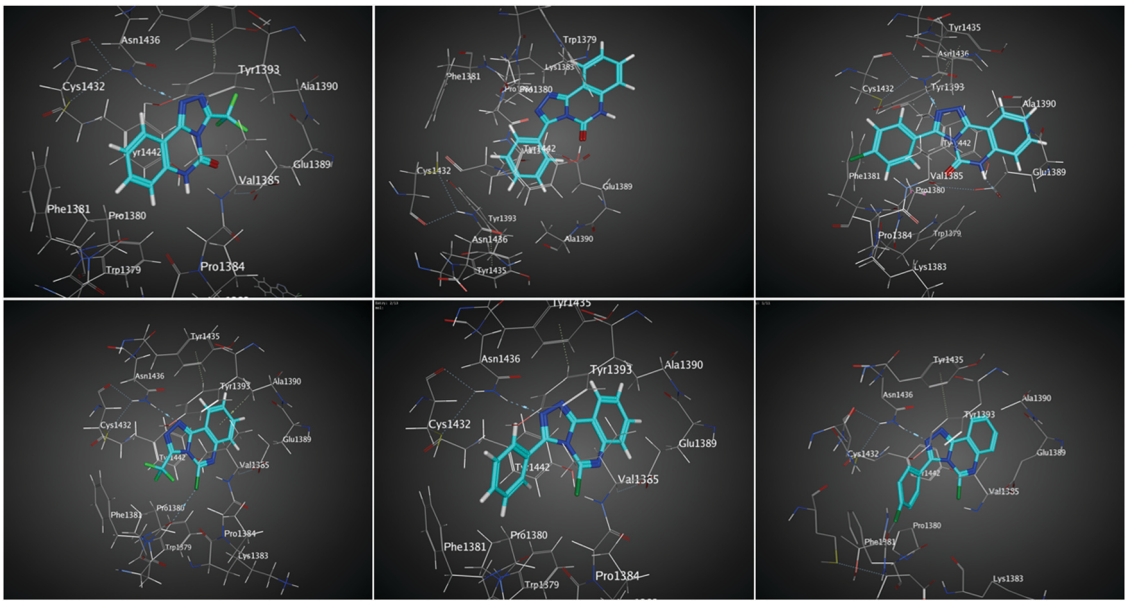

Fig. 7 3D binding interactions of **21** (upper left), **22** (upper middle), **23** (upper right), **24** (lower left), **25** (lower middle), and **26** (lower right) with the active site of histone acetyltransferase PfGCN5 (homologous Brd with PCAF).

2.5. *In silico* pharmacokinetic study

A computational study was conducted for the compounds that showed the best *in vitro* anticancer activity to evaluate their physicochemical properties according to the directions of Lipinski's rule of five.[46] According to the Lipinski rule, the intestinal absorption of a molecule is predicted to be acceptable if it fulfills four rules: (i) molecular weight < 500; (ii) number of H bond donors ≤ 5; (iii) number of H bond acceptors ≤ 10; and (iv) $\log P < 5$. Also, reduced molecular flexibility (as indicated by the count of rotatable bonds), a low polar surface area, and the total count of hydrogen bond donors and acceptors are found to be crucial predictors of good oral bioavailability.[47] In this study, the reference anticancer drug was found to violate three of Lipinski's rules while bromosporine and all the designed bioisosteres pleasingly satisfied all Lipinski's rules. For all the new ligands, the numbers of hydrogen bond acceptor and donor groups are within the acceptable range (4 and ≤ 1, respectively). The molecular weights of and the total count of rotatable bonds in the new ligands are much lower than those of doxorubicin and bromosporine. Additionally, the ADMET profiles of the new triazoloquinazolines were tentatively investigated to evaluate their potential to build up as new oral drug candidates. This study has been performed with the aid of the pkCSM descriptors algorithm.[48]

Drug absorption depends on many factors including intestinal absorption, membrane and skin permeabilities, and being a P-glycoprotein substrate or inhibitor. The distribution of a drug depends on the volume of distribution (VDss), the blood brain barrier permeability (logBB), and the CNS permeability. Metabolism is predicted depending on the CYP inhibition. Excretion is predicted based on the total clearance and the renal OCT2 substrate. The toxicity of the drugs is predicted depended on the AMES toxicity, hERG I & II inhibition, hepatotoxicity, and skin sensitization. All parameters were studied for the best effective new derivatives as well as to the reference anticancer and PCAF inhibitory agents. From the obtained data shown in Table 3, we can suggest that the new derivatives are predicted to possess superior intestinal absorption in humans over all the reference drugs (92.59–97.68) compared with 62.37 and 82.25 in the case of doxorubicin and bromosporine. This advantage may be attributed to the superior lipophilicity of the new compounds, which would make them have significant good bioavailability after oral administration.[49]

In regards to the CNS permeability, our newly designed L-45 bioisosteres are suggested to have a higher possibility to penetrate the CNS (CNS permeability 2.28 to -1.39 compared with -4.30 for doxorubicin and -3.27 for bromosporine). It is also obvious that CYP3A4, the key enzyme in the metabolism, could be inhibited under the effect of bromosporine and five of the new triazoloquinazolines (**22**, **23**, **24**, **25**, and **26**). This is possibly due to the relatively higher lipophilicity of our new ligands. Excretion was predicted based on the total clearance, a substantial parameter in determining dose intervals. The tabulated results revealed that bromosporine and its newly designed bioisosteres have comparable total clearance values (-0.03 to 0.78) which are much lower than that of doxorubicin. Thus, doxorubicin could be excreted faster and consequently needs shorter dosing intervals. Dissimilar to doxorubicin, all other compounds are predicted to exhibit much slower clearance rates, which suggests the preference of possible longer dosing intervals for bromosporine and the new compounds.

Toxicity is the last parameter analyzed in the pharmacokinetic profiles of our newly synthesized derivatives. As presented in Table 3, all the new derivatives except **26** shared the disadvantage of expected AMES toxicity, which indicates the drawback of probable mutagenic potential of these compounds.[50]

Table 3 ADMET profile of the six most active derivatives and reference anticancer and PCAF inhibitory agents

Parameter	**21**	**22**	**23**	**24**	**25**	**26**	Doxorubicin	Bromosporine
Molecular properties								
Molecular weight	254.171	262.272	296.717	272.617	280.718	315.163	543.525	404.452
log *P*	1.5896	2.2378	2.8912	2.9497	3.5979	4.2513	0.0013	2.34804
Rotatable bonds	0	1	1	0	1	1	5	5
HB acceptors	4	4	4	4	4	4	12	8
HB donors	1	1	1	0	0	0	6	2
Surface area	96.882	113.077	123.381	103.023	119.219	129.522	222.081	161.528
Absorption								
Water solubility	−4.042	−3.398	−3.509	−3.711	−3.458	−3.611	−2.915	−3.035
Caco2 permeability	0.523	0.734	0.829	1.751	1.607	1.458	0.457	0.703
Intestinal abs. (human)	92.599	96.169	94.648	93.989	97.685	96.101	62.372	82.254
Skin permeability	−3.032	−2.753	−2.757	−2.582	−2.731	−2.729	−2.735	−2.737
P-Glycoprotein substrate	No	Yes	Yes	No	No	No	Yes	No
P-Glycoprotein I inhibitor	No	No	No	No	No	No	No	Yes
P-Glycoprotein II inhibitor	No	No	No	No	Yes	Yes	No	No
Distribution								
VDss (human)	−0.378	−0.2	−0.116	−0.304	0.095	0.187	1.647	−0.361
Fraction unbound (human)	0.321	0.133	0.144	0.223	0.248	0.26	0.215	0.116
BBB permeability	0.449	0.58	0.535	0.918	1.011	0.965	−1.379	−1.473
CNS permeability	−2.28	−2.097	−1.98	−1.664	−1.4	−1.396	−4.307	−3.277
Metabolism								
CYP2D6 substrate	No	No	No	No	No	No	No	No
CYP3A4 substrate	No	Yes	Yes	Yes	Yes	Yes	No	Yes
CYP1A2 inhibitor	Yes	Yes	Yes	Yes	Yes	Yes	No	No
CYP2C19 inhibitor	No	No	Yes	Yes	Yes	Yes	No	No
CYP2C9 inhibitor	No	No	Yes	No	Yes	Yes	No	No
CYP2D6 inhibitor	No	No	No	No	No	No	No	No
CYP3A4 inhibitor	No	Yes	Yes	No	No	No	No	No
Excretion								
Total clearance	0.27	0.784	−0.038	0.133	0.215	−0.035	0.987	0.022
Renal OCT2 substrate	No	No	No	No	No	No	No	No
Toxicity								
AMES toxicity	Yes	Yes	Yes	Yes	Yes	No	No	No
Max. tolerated dose	−0.2	0.407	0.389	−0.079	0.535	0.442	0.081	0.606
hERG I inhibitor	No	No	No	No	No	No	No	No
hERG II inhibitor	No	Yes	Yes	No	No	No	Yes	Yes
Oral rat acute toxicity (LD_{50})	2.613	2.749	2.753	2.713	2.436	2.458	2.408	2.148
Oral rat chronic toxicity (LOAEL)	1.367	1.368	1.308	1.642	0.853	0.675	3.339	1.783
Hepatotoxicity	Yes	Yes	Yes	Yes	Yes	Yes	Yes	Yes
Skin sensitization	No	No	No	No	No	No	No	No
T. Pyriformis toxicity	0.606	0.31	0.315	0.5	0.293	0.296	0.285	0.287
Minnow toxicity	1.661	0.618	0.143	0.693	−0.048	−0.914	4.412	0.952

Conversely, **26** is expected to be non-mutagenic as revealed from the test of AMES toxicity. However, they are expected to not inhibit hERG I activity. This inability suggests their safety for human heart electrical activity.[51] Unfortunately, two of the new L-45 bioisosteres are expected to share the disadvantage of both doxorubicin and bromosporine as they could inhibit hERG II, which indicates the probability of cardiac arrhythmia risk. In addition, all the triazoloquinazolines, doxorubicin, and bromosporine shared the drawback of expected hepatotoxicity. In regard to the maximum tolerated dose in humans, four of the new ligands (**21**, **22**, **24**, and **25**) are suggested to have intermediate tolerability between that of doxorubicin and bromosporine, which means the advantage of wide therapeutic indices of these derivatives. Additionally, all the designed L-45 bioisosteres are expected to show lower Minnow toxicity values than that of doxorubicin. These lower values of Minnow toxicities disclosed the lower predicted risk of the new bioisosteres in the aquatic environment.[52] Finally, the oral acute toxic doses (LD_{50}) of the new compounds are expected to be almost equal to or even a little higher than those of the reference anticancer and PCAF inhibitory agents.

3. Conclusion

In conclusion, this work reports a bioisosteric guided approach for the design of a novel series of triazoloquinazolines derivatives as analogous structures of the first reported triazolophthalazine PCAF inhibitor, L-45, with the objective of identifying new PCAF inhibitors with potential anticancer activity. The target bioisosteres were designed based on keeping essential structural fragments that are essential for binding with the PCAF receptor

binding site with three structural modifications of the lead compound. First, the pyrimidine ring replaced the pyridazine ring of L-45 to keep the favorable π–π stacking interaction with the Tyr1442 residue. Second, different substitution patterns were introduced to position 5 of triazoloquinazoline scaffolds to investigate the effect on the cytotoxic activity. Last, the methyl group at C-3 of L-45 was replaced by three different substituent groups of different electronic and spatial characteristics. Six of our designed bioisosteres showed moderate to good cytotoxic effects against four human cancer cell lines (HePG2, MCF-7, PC3, and HCT-116). Among which, compounds **21** and **23** were the most potent against all the tested cancer cell lines, with IC_{50} values in the range of 5.93–9.58 μM. Additionally, molecular docking, SAR, and *in silico* pharmacokinetic prediction studies were conducted. The results of these studies verified the good activities of both compounds by anticipating potential binding interactions with the active site of histone acetyltransferase. The *in silico* ADMET profiling study indicated that the designed bioisosteres presented promising pharmacokinetic profiles. Overall, the most active candidates in the quest for effective cytotoxic agents will serve as useful leads and merit further investigation.

4. Experimental section

4.1. General

Melting points were measured using an electrothermal (Stuart SMP30) apparatus and were uncorrected. Infrared spectra were recorded on a Pye Unicam SP 1000 IR spectrophotometer at the Pharmaceutical Analytical Unit, Faculty of Pharmacy, Al-Azhar University. ^{1}H NMR and ^{13}C NMR spectra were recorded in DMSO-d_6 at 300 and 100 MHz, respectively, on a Varian Mercury VXR-300 NMR spectrometer at the NMR Lab, Faculty of Science, Cairo University. TMS was used as an internal standard, and chemical shift and coupling constant values are listed in ppm and Hz, respectively. Mass spectra and elemental analyses were carried out at the Regional Center of Mycology and Biotechnology, Al-Azhar University, Cairo, Egypt. The reaction progress was monitored with Merck silica gel IB2-F plates (0.25 mm thickness) visualized under a UV lamp using different solvent systems as mobile phases. The reagents and starting compounds anthranilic acid, phosphorus oxychloride, hydrazine, acid anhydrides, and amine derivatives were purchased from the Aldrich chemical company and were used as received. Compounds **25** and **26** were synthesized according to the directions of previously reported procedures.[38]

4.2. General procedure for synthesis of 3-substituted-[1,2,4]triazolo[4,3-*c*]quinazolin-5(6*H*)-one (21–23)

Into a stirred solution of 2-chloro-4-hydrazinylquinazoline **20** (0.194 g, 0.001 mol) in glacial acetic acid (20 ml), the appropriate acid halide (0.001 mole) was added. The reaction mixture was heated to reflux temperature in a water bath for 6 hours. After cooling to room temperature, the reaction mixture was poured into ice-cooled water (100 ml) and stirred for one more hour. The formed precipitate was filtered off under a vacuum and washed with a copious amount of water (50 ml), and then finally recrystallized from methanol to afford the corresponding triazoloquinazolinone derivative.

4.2.1. 3-(Trifluoromethyl)-[1,2,4]triazolo[4,3-*c*]quinazolin-5(6*H*)-one (21).

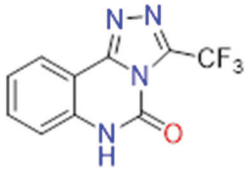

Greenish white solid, yield: 95%; m.p. 259–261 °C. IR (KBr) cm^{-1}: 3163 (NH), 3059 (CH aromatic), 1697 (C═O), 1597 (C═C aromatic). ^{1}H NMR (DMSO-d_6) δ ppm: 11.19 (s, 1H, NH, D_2O exchangeable), 7.93 (d, J = 8.4 Hz, 1H, quinazoline-H10), 7.66 (dd, J = 7.6 Hz, 1H, quinazoline-H8), 7.39 (d, J = 5.2 Hz, 1H, quinazoline-H7), 7.22 (dd, J = 8.4 Hz, 1H, quinazoline-H9). MS (m/z): 254 ($C_{10}H_5F_3N_4O$), 237 ($C_{10}H_4F_3N_4$, 6.71%). Anal. calc. for ($C_{10}H_5F_3N_4O$) (M.W. = 254): C, 47.25; H, 1.98; N, 22.04%; found: C, 47.49; H, 2.16; N, 22.21%.

4.2.2. 3-Phenyl-[1,2,4]triazolo[4,3-*c*]quinazolin-5(6*H*)-one (22).

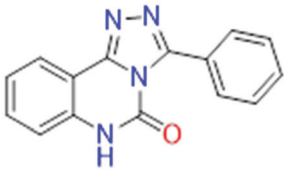

Yellowish green solid, yield: 88%; m.p. 269–271 °C. IR (KBr) cm^{-1}: 3205 (NH), 3051 (CH aromatic), 1678 (C═O), 1624 (C═C aromatic). ^{1}H NMR (DMSO-d_6) δ ppm: 11.41 (s, 1H, NH, D_2O exchangeable), 7.96 (d, 2H, phenyl-H2, H6), 7.88 (d, J = 8.4 Hz, 1H, quinazoline-H10), 7.64 (dd, J = 7.6 Hz, 1H, quinazoline-H8), 7.42 (dd, J = 7.6 Hz, 3H, phenyl-H3, H4, H5), 7.20 (d, J = 8.4 Hz, 1H, quinazoline-H7), 7.19 (dd, J = 8.4 Hz, 1H, quinazoline-H9). ^{13}C NMR (DMSO-d_6) δ ppm: 161.95 (triazole-C3), 135.09 (quinazoline-C═O), 135.01 (quinazoline-C4), 134.18 (quinazoline-C8a), 131.87 (phenyl-C1), 130.02 (phenyl-C4), 129.39 (phenyl-C3, C5), 129.03 (quinazoline-C8), 128.98 (phenyl-C2, C6), 128.83 (quinazoline-C6), 127.92 (quinazoline-C5), 127.01 (quinazoline-C8) and 122.96 (quinazoline-C8a). MS (m/z): 262 ($C_{15}H_{10}N_4O$, 11.64%), 63 (100%). Anal. calc. for ($C_{15}H_{10}N_4O$) (M.W. = 262): C, 68.69; H, 3.84; N, 21.36%; found: C, 68.92; H, 4.09; N, 21.54%.

4.2.3. 3-(4-Chlorophenyl)-[1,2,4]triazolo[4,3-*c*]quinazolin-5(6*H*)-one (23).

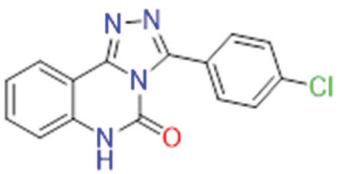

Yellowish white solid, yield: 82%; m.p. 282–284 °C. IR (KBr) cm^{-1}: 3225 (NH), 3045 (CH aromatic), 1674 (C═O),

1626 (C═C aromatic). ^{1}H NMR (DMSO-d_6) δ ppm: 11.43 (s, 1H, NH, D_2O exchangeable), 7.96 (d, 2H, phenyl-H2, H6), 7.88 (d, J = 8.4 Hz, 1H, quinazoline-H10), 7.64 (dd, J = 7.60 Hz, 1H, quinazoline-H8), 7.41 (dd, J = 7.6 Hz, 2H, phenyl-H3, H5), 7.21 (d, J = 8.4 Hz, 1H, quinazoline-H7), 7.19 (dd, J = 8.4 Hz, 1H, quinazoline-H9). ^{13}C NMR (DMSO-d_6) δ ppm: 160.95 (triazole-C3), 135.08 (quinazoline-C═O), 135.00 (quinazoline-C4), 134.17 (quinazoline-C8a), 131.86 (phenyl-C1), 130.01 (phenyl-C4), 129.36 (phenyl-C3, C5), 129.01 (quinazoline-C8), 128.97 (phenyl-C2, C6), 128.82 (quinazoline-C6), 127.91 (quinazoline-C5), 127.02 (quinazoline-C8) and 122.97 (quinazoline-C8a). MS (m/z): 296 ($C_{15}H_9ClN_4O$), 296 ($C_{15}H_9N_4O$, 100%). Anal. calc. for ($C_{15}H_{10}N_4O$) (M.W. = 262): C, 68.69; H, 3.84; N, 21.36%; found: C, 68.92; H, 4.09; N, 21.54%.

4.3. General procedure for synthesis of 5-chloro-3-(substituted)-[1,2,4]triazolo[4,3-*c*]quinazoline (24–26)

The appropriate 3-(4-chlorophenyl)-[1,2,4]triazolo[4,3-*c*]quinazolin-5(6*H*)-one (**21–23**) (0.001 mol) in posphorusoxy chloride (10 ml) was heated to reflux temperature in a water bath for 7–8 hours. After cooling to room temperature, the reaction mixture was quenched in ice-cooled water (100 ml). The obtained solid was filtered off under a vacuum and washed with a copious amount of water (50 ml), dried, and finally recrystallized from ethanol to afford the corresponding 5-chloro-3-(substituted)-[1,2,4]triazolo[4,3-*c*]quinazoline derivative.

4.3.1. 5-Chloro-3-(trifluoromethyl)-[1,2,4]triazolo[4,3-*c*]-quinazoline (24).

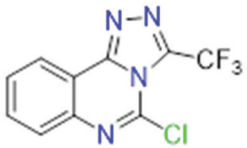

Yellowish white solid, yield: 73%; m.p. 266–268 °C. IR (KBr) cm^{-1}: 3056 (CH aromatic), 2847 (CH aliphatic), 1619 (C═C aromatic). ^{1}H NMR (DMSO-d_6) δ ppm: 7.87 (d, J = 8 Hz, 1H, quinazoline-H10), 7.63 (dd, J = 7.6 Hz, 1H, quinazoline-H8), 7.17–7.19 (d, J = 8.4 Hz, 1H, quinazoline-H7), 7.15 (dd, J = 8.4 Hz, 1H, quinazoline-H9). MS (m/z): 274 ($C_{10}H_4ClF_3N_4$, 4.99%, M^{2+}), 272 ($C_{10}H_4ClF_3N_4$, 64.57%), 168 ($C_9H_4N_4$, 1.47%). Anal. calc. for ($C_{10}H_4ClF_3N_4$) (M.W. = 272): C, 44.06; H, 1.48; N, 20.55%; found: C, 44.32; H, 1.72; N, 20.38%.

4.3.2. 5-Chloro-3-phenyl-[1,2,4]triazolo[4,3-*c*]quinazoline (25)[38].

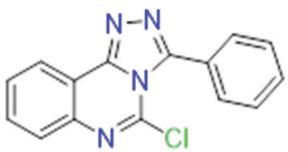

Greenish white solid, yield: 80%; m.p. 143–145 °C. IR (KBr) cm^{-1}: 3081 (CH aromatic), 1620 (C═N). MS (m/z): 280 ($C_{15}H_9ClN_4$), 280 ($C_{15}H_9ClN_4$, M +, 100%), 282 ($C_{15}H_9ClN_4$, M + 2, 31.08%). Anal. calc. for ($C_{15}H_{10}N_4O$) (M.W. = 280): C, 64.18; H, 3.23; N, 19.96%; found: C, 64.20; H, 3.20; N, 20.01%.

4.3.3. 5-Chloro-3-(4-chlorophenyl)-[1,2,4]triazolo[4,3-*c*]-quinazoline (26)[38].

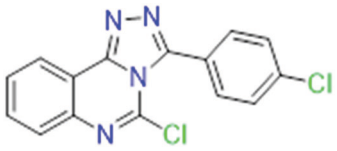

Yellowish white solid, yield: 65%; m.p. 226–228 °C. IR (KBr) cm^{-1}: 3092 (CH aromatic), 1621 (C═N). MS (m/z): 315 ($C_{15}H_8C_2lN_4$), 315 ($C_{15}H_8C_2lN_4$, 100%), 317 ($C_{15}H_8C_2lN_4$, M + 2, 32.17%). Anal. calc. for ($C_{15}H_{10}N_4O$) (M.W. = 280): C, 57.17; H, 2.56; N, 22.50%; found: C, 57.21; H, 2.56; N, 22.59%.

4.4. General procedure for synthesis of 4-(3-(substituted)-[1,2,4]triazolo[4,3-*c*]quinazolin-5-yl)amine derivatives (27–36)

Into a solution of the appropriate 5-chloro-[1,2,4]triazolo-[4,3-*c*]quinazoline derivative (**24–26**) (0.001 mol) in isopropyl alcohol (20 ml), an equimolar amount of the appropriate amine was added. The reaction mixture was heated to reflux at 120 °C overnight. After cooling to room temperature, the reaction mixture was quenched in ice-cooled water (100 ml). The obtained solid was filtered off under reduced pressure and washed with water (50 ml), dried, and finally recrystallized from ethanol.

4.4.1. 4-(3-(Trifluoromethyl)-[1,2,4]triazolo[4,3-*c*]quinazolin-5-yl)morpholine (27).

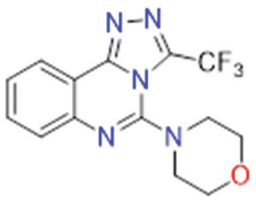

Yellowish solid, yield: 78%; m.p. 262–264 °C. IR (KBr) cm^{-1}: 3032 (CH aromatic), 2962 (CH aliphatic), 1612 (C═N), 1566 (C═C aromatic).^{1}H NMR (DMSO-d_6) δ ppm: 7.79 (d, 1H, J = 4 Hz, quinazoline-H7), 7.58 (dd, 1H, J = 12 Hz, quinazoline-H8), 7.40 (d, 1H, J = 4 Hz, quinazoline-H10), 7.13 (dd, 1H, J = 4 Hz, quinazoline-H9), 3.66 (t, 4H, J = 4 Hz, $(CH_2)_2N$), 3.60 (t, 4H, J = 4 Hz, $(CH_2)_2O$). MS (m/z): 323 ($C_{14}H_{12}F_3N_5O$, 8.17%, M^+), 304 ($C_{14}H_{12}F_2N_5O$ 9.78%), 269 ($C_{14}H_{12}F_1N_5$, 100%). Anal. calc. for ($C_{14}H_{12}F_3N_5O$) (M.W. = 323): C, 52.01; H, 3.74; N, 21.66%; found: C, 52.27; H, 3.87; N, 21.85%.

4.4.2. 5-(Piperazin-1-yl)-3-(trifluoromethyl)-[1,2,4]triazolo-[4,3-*c*]quinazoline (28).

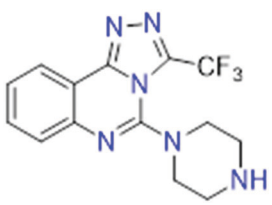

Faint brown solid, yield: 76%; m.p. 258–260 °C. IR (KBr) cm^{-1}: 3422 (NH), 3065 (CH aromatic), 2925 (CH aliphatic), 1609 (C═N), 1551 (C═C aromatic). ^{1}H NMR (DMSO-d_6) δ ppm:

8.14 (d, 1H, J = 8 Hz, quinazoline-H7), 7.99 (dd, 1H, J = 7.7 Hz, quinazoline-H8), 7.46 (d, 1H, J = 8.4 Hz, quinazoline-H10), 7.71 (dd, 1H, J = 8.4 Hz, quinazoline-H9), 3.88 (t, 4H, $(CH_2)_2$–N), 2.81 (t, 4H, $(CH_2)_2$–NH), 1.29 (s, 1H, NH). MS (m/z): 322 ($C_{14}H_{13}F_3N_6$, 23.01%, M^+), 278 ($C_{12}H_7F_3N_5$, 23.70%), 264 ($C_{11}H_5F_3N_5$, 9.53%), 57 (C_3H_7N, 100%). Anal. calc. for ($C_{14}H_{13}F_3N_6$) (M.W. = 322): C, 52.17; H, 4.07; N, 26.08%; found: C, 52.40; H, 4.28; N, 25.91%.

4.4.3. *N*-Butyl-3-phenyl-[1,2,4]triazolo[4,3-*c*]quinazolin-5-amine (29).

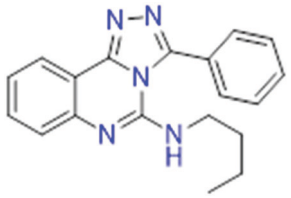

Faint greenish white solid, yield: 62%; m.p. 267–269 °C. IR (KBr) cm^{-1}: 3331 (NH), 3059 (CH aromatic), 2958 (CH aliphatic), 1627 (C═N), 1524 (C═C aromatic). ^{1}H NMR (DMSO-d_6) δ ppm: 8.05 (d, 1H, J = 8 Hz, quinazoline-H7), 7.88 (d, 1H, J = 8.4 Hz, quinazoline-H10), 7.81 (s, 1H, NH), 7.52 (dd, 2H, J = 8 Hz, phenyl-H2, H6), 7.43 (dd, 1H, J = 8.4 Hz, quinazoline-H8), 7.42 (dd, 1H, J = 8.4 Hz, quinazoline-H9), 7.04 (dd, 3H, J = 8 Hz, phenyl-H3, H4, H5), 3.35 (t, 2H, CH_2–NH), 1.51 (m, 2H, CH_2), 1.35 (m, 2H, CH_2), 0.93 (t, 3H, J = 8 Hz, CH_3). MS (m/z): 317 ($C_{19}H_{19}N_5$, 8.23%, M^+), 262 ($C_{16}H_{14}N_4$, 1.62%), 77 (C_6H_5, 100%). Anal. calc. for ($C_{19}H_{19}N_5$) (M.W. = 317): C, 71.90; H, 6.03; N, 22.07%; found: C, 63.87; H, 4.95; N, 20.91%.

4.4.4. 3-Phenyl-5-(piperazin-1-yl)-[1,2,4]triazolo[4,3-*c*]-quinazoline (30).

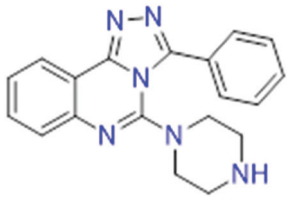

Yellowish white solid, yield: 73%; m.p. 251–253 °C. IR (KBr) cm^{-1}: 3422 (NH), 3066 (CH aromatic), 2925 (CH aliphatic), 1610 (C═N), 1551 (C═C aromatic). 1H NMR (DMSO-d_6) δ ppm: 8.13 (dd, 2H, J = 8 Hz, phenyl-H2, H6), 8.07 (d, 1H, J = 8 Hz, quinazoline-H10), 7.65 (dd, 1H, J = 7.7 Hz, quinazoline-H9), 7.61 (dd, 3H, J = 8 Hz, phenyl-H3, H4, H5), 7.56 (d, 1H, J = 8.4 Hz, quinazoline-H7), 7.19 (dd, 1H, J = 8.4 Hz, quinazoline-H8), 3.21 (t, 4H, $(CH_2)_2$N), 2.39 (t, 4H, $(CH_2)_2$NH), 1.21 (s, 1H, NH). MS (m/z): 330 ($C_{19}H_{18}N_6$, 32.42%, M^+), 77 (C_6H_5, 100%). Anal. calc. for ($C_{19}H_{18}lN_6$) (M.W. = 330): C, 69.07; H, 5.49; N, 25.44%; found: C, 69.15; H, 5.71; N, 25.16%.

4.4.5. 4-(3-(4-Chlorophenyl)-[1,2,4]triazolo[4,3-*c*]quinazolin-5-yl)morpholine (31).

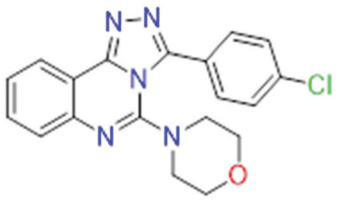

White solid, yield: 69%; m.p. 269–271 °C. IR (KBr) cm^{-1}: 3075 (CH aromatic), 2974 (CH aliphatic), 1625 (C═N), 1552 (C═C aromatic). ^{1}H NMR (DMSO-d_6) δ ppm: 8.42 (d, 1H, J = 7.2 Hz, quinazoline-H7), 8.26 (d, 1H, J = 8.4 Hz, quinazoline-H10), 8.02 (dd, 2H, J = 8, phenyl-H2, H6), 7.65 (dd, 2H, J = 8, phenyl-H3, H5), 7.42 (dd, 1H, J = 7.7 Hz, quinazoline-H8), 7.12 (dd, 1H, J = 8.4 Hz, quinazoline-H9), 3.68 (t, 4H, J = 8.4 Hz, $(CH_2)_2$N), 3.57 (t, 4H, J = 4.5 Hz, $(CH_2)_2$O). ^{13}C NMR (DMSO-d_6) δ ppm: 162.34 (quinazoline-C2), 157.80 (quinazoline-C4), 154.98 (triazole-C3), 138.82 (quinazoline-C8a), 135.62 (phenyl-C4), 134.80 (quinazoline-C7), 129.02 (phenyl-C1), 127.63 (phenyl-C2, C6), 124.63 (phenyl-C3, C5), 120.00 (quinazoline-C8), 116.70 (quinazoline-C5), 115.18 (quinazoline-C6), 110.79 (quinazoline-C4a), 67.00, (CH_2OCH_2), 45.89 (CH_2NCH_2). MS (m/z): 367 ($C_{19}H_{16}ClN_5O$, M^{2+}), 365 ($C_{19}H_{16}ClN_5O$, M^+, 38.19%), 337 ($C_{17}H_{12}ClN_5O$, 12.67%), 296 ($C_{15}H_9ClN_4O$, 23.55%). Anal. calc. for ($C_{19}H_{16}ClN_5O$) (M.W. = 365): C, 62.38; H, 4.41; N, 19.14%; found: C, 62.59; H, 4.38; N, 19.95%.

4.4.6. 3-(4-Chlorophenyl)-*N*-ethyl-[1,2,4]triazolo[4,3-*c*]quinazolin-5-amine (32).

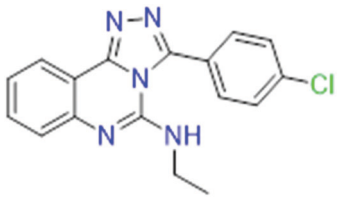

White solid, yield: 69%; m.p. 259–261 °C. IR (KBr) cm^{-1}: 3232 (NH), 3078 (CH aromatic), 2931 (CH aliphatic), 1624 (C═N), 1558 (C═C aromatic). ^{1}H NMR (DMSO-d_6) δ ppm: 7.83 (s, 1H, NH, D_2O exchangeable), 7.73 (d, 1H, J = 7.2 Hz, quinazoline-H7), 7.71 (d, 1H, J = 8.4 Hz, quinazoline-H10), 7.66 (dd, 2H, J = 8 Hz, phenyl-H2, H6), 7.59 (dd, 1H, J = 7.7 Hz, quinazoline-H8), 7.46 (dd, 1H, J = 8.4 Hz, quinazoline-H9), 7.40 (dd, 2H, J = 8 Hz, phenyl-H3, H5), 3.18 (q, 2H, CH_2–NH), 1.11 (t, 3H, J = 8.4 Hz, CH_3). MS (m/z): 325 ($C_{17}H_{14}ClN_5$, 12.82%, M^+ + 2), 323 ($C_{17}H_{14}ClN_5$, 41.8%, M^+), 294 ($C_{15}H_9$ ClN_5, 20.21%). Anal. calc. for ($C_{17}H_{14}ClN_5$) (M.W. = 323): C, 63.06; H, 4.36; N, 21.63%; found: C, 63.28; H, 4.50; N, 21.49%.

4.4.7. 3-(4-Chlorophenyl)-*N*-propyl-[1,2,4]triazolo[4,3-*c*]quinazolin-5-amine (33).

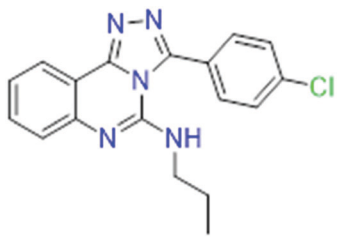

Yellowish brown solid, yield: 60%; m.p. 262–264 °C. IR (KBr) cm^{-1}: 3421 (NH), 3078 (CH aromatic), 2960 (CH aliphatic), 1628 (C═N), 1544 (C═C aromatic). ^{1}H NMR (DMSO-d_6) δ ppm: 8.34 (d, 1H, J = 8 Hz, quinazoline-H7), 8.18 (dd, 2H, J = 8 Hz, phenyl-H2, H6), 8.12 (d, 1H, J = 8.4 Hz, quinazoline-H10), 7.80 (dd, 1H, J = 7.7 Hz, quinazoline-H8), 7.74 (dd, 2H, J = 8 Hz, phenyl-H3,

H5), 7.70 (s, 1H, NH), 7.65 (dd, 1H, J = 8.4 Hz, quinazoline-H9), 3.58 (t, 2H, J = 8.4, CH_2–NH), 1.27 (m, 2H, CH_2), 0.92 (t, 3H, J = 8.0, CH_3). MS (m/z): 339 ($C_{18}H_{16}ClN_5$, 9.50%, M^+ + 2), 337 ($C_{18}H_{16}ClN_5$, 24.77%, M^+), 322 ($C_{17}H_{13}ClN_5$, 3.00%), 308 ($C_{16}H_{11}ClN_5$, 7.07%), 294 ($C_{15}H_9ClN_5$, 29.36%), 279 ($C_{15}H_8ClN_4$, 2.70%). Anal. calc. for ($C_{18}H_{16}ClN_5$) (M.W. = 337): C, 64.00; H, 4.77; N, 20.73%; found: C, 63.87; H, 4.95; N, 20.91%.

4.4.8. *N*-benzyl-3-(4-chlorophenyl)-[1,2,4]triazolo[4,3-*c*]quinazolin-5-amine (34).

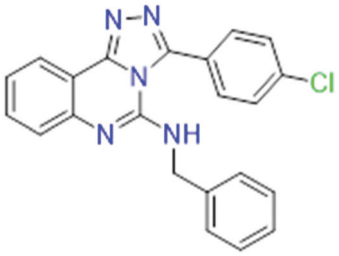

Yellowish white solid, yield: 74%; m.p. 268–270 °C. IR (KBr) cm^{-1}: 3295 (NH), 3061 (CH aromatic), 2927 (CH aliphatic), 1621 (C═N), 1548 (C═C aromatic). ^{1}H NMR (DMSO-d_6) δ ppm: 8.30 (d, 1H, J = 8 Hz, quinazoline-H7), 8.22 (dd, 2H, J = 8 Hz, phenyl-H2, H6), 8.00 (d, 1H, J = 8.4 Hz, quinazoline-H10), 7.78 (dd, 1H, J = 4 Hz, quinazoline-H8), 7.38 (dd, 2H, J = 8 Hz, phenyl-H3, H5), 7.26 (m, 5H, benzylic protons), 7.24 (s, 1H, NH, D_2O exchangeable), 7.09 (dd, 1H, J = 8.4 Hz, quinazoline-H9), 4.35 (s, 2H, CH_2–NH). ^{13}C NMR (DMSO-d_6) δ ppm: 157.74 (quinazoline-C2), 155.69 (quinazoline-C4), 140.86 (triazole-C3), 139.02 (quinazoline-C8a), 134.52 (benzylic-C1), 130.31 (phenyl-C4), 129.32 (quinazoline-C8), 128.72 (phenyl-C1), 128.51 (phenyl-C2, C6), 127.88 (phenyl-C3, C5), 127.54 (benzylic-C3, C5), 127.13 (benzylic-C2, C4, C6), 121.40 (quinazoline-C6, C7), 120.57 (quinazoline-C5), 115.50 (quinazoline-C4a), and 43.39 (CH_2NH). MS (m/z): 387 ($C_{22}H_{16}ClN_5$, 20.90%, M^+ + 2), 385 ($C_{22}H_{16}ClN_5$, 46.40%, M^+), 274 ($C_{16}H_{12}N_5$, 29.42%), 196 ($C_{10}H_6N_5$, 16.08%). Anal. calc. for ($C_{22}H_{16}ClN_5$) (M.W. = 385): C, 68.48; H, 4.18; N, 18.15%; found: C, 68.61; H, 4.42; N, 17.98%.

4.4.9. 1-{4-[(3-(4-Chlorophenyl)-[1,2,4]triazolo[4,3-*c*]quinazolin-5-yl)amino]phenyl}ethan-1-one (35).

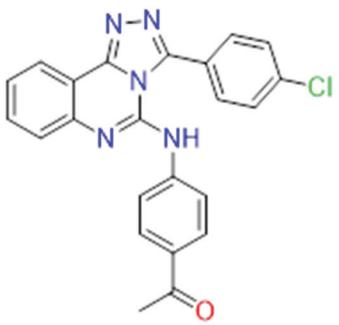

Faint brown solid, yield: 66%; m.p. 263–265 °C. IR (KBr) cm^{-1}: 3182 (NH), 3050 (CH aromatic), 2924 (CH aliphatic), 1752 (C═O), 1625 (C═N), 1598 (C═C aromatic). ^{1}H NMR (DMSO-d_6) δ ppm: 12.34 (S, 1H, NH, D_2O exchanged), 8.29 (dd, 2H, J = 8 Hz, phenyl-H2, H6), 8.20 (dd, 2H, J = 8 Hz, *p*-aminoacetophenone-H3, H5), 8.14 (d, 1H, J = 8 Hz, quinazoline-H7), 7.99 (dd, 1H, J = 7.7 Hz, quinazoline-H8), 7.71 (dd, 1H, J = 8.4 Hz, H9 quinazoline-H9), 7.63 (dd, 2H, J = 8 Hz, phenyl-H3, H5), 7.46 (d, 1H, J = 8.4 Hz, quinazoline-H10), 7.39 (dd, 2H, J = 8 Hz, *p*-aminoacetophenone-H2, H6), 2.42 (s, 3H, CH_3). ^{13}C NMR (DMSO-d_6) δ ppm: 162.34 (C═O), 153.89 (quinazoline-C2), 144.23 (quinazoline-C4), 137.51 (triazole-C3), 135.59 (quinazoline-C8a), 133.27 (*p*-amino acetophenone-C1), 132.27 (phenyl-C1), 129.53 (quinazoline-C7), 129.05 (phenyl-C3, C5), 128.95 (*p*-amino acetophenone-C2–C6), 124.58 (phenyl-C2, C4, C6), 124.04 (quinazoline-C5, C6), 116.54 (quinazoline-C4a), 110,68 (quinazoline-C8), and 25.92 (CH3). MS (m/z): 415 ($C_{23}H_{16}ClN_5O$, 3.68%, M^+ + 2), 413 ($C_{23}H_{16}ClN_5$ O, 10.78%, M^+), 399 ($C_{22}H_{14}ClN_5O$, 1.51%), 371 ($C_{21}H_{14}ClN_5$, 1.69%), 295 ($C_{15}H_{10}ClN_5$, 6.16%). Anal. calc. for ($C_{23}H_{16}ClN_5O$) (M.W. = 413): C, 66.75; H, 3.90; N, 16.92%; found: C, 66.91; H, 4.17; N, 17.05%.

4.4.10. 3-(4-Chlorophenyl)-5-(piperazin-1-yl)-[1,2,4]triazolo-[4,3-*c*]quinazoline (36).

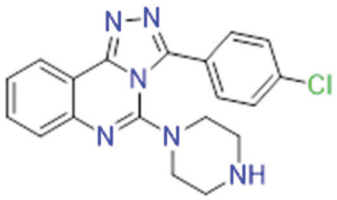

Yellowish white solid, yield: 81%; m.p. 254–256 °C. IR (KBr) cm^{-1}: 3451 (NH), 3050 (CH aromatic), 2924 (CH aliphatic), 1626 (C═N), 1555 (C═C aromatic). ^{1}H NMR (DMSO-d_6) δ ppm: 8.33 (d, 1H, J = 8 Hz, quinazoline-H10), 8.18 (dd, 2H, J = 8 Hz, phenyl-H2, H6), 7.85 (dd, 1H, J = 7.7 Hz, quinazoline-H9), 7.70 (d, 1H, J = 8.4 Hz, quinazoline-H7), 7.64 (dd, 2H, J = 8 Hz, phenyl-H3, H5), 7.39 (dd, 1H, J = 8.4 Hz, quinazoline-H8), 3.36 (t, 4H, $(CH_2)_2$-N), 2.84 (t, 4H, $(CH_2)_2$-NH), 1.29 (s, 1H, NH). MS (m/z): 366 ($C_{19}H_{17}ClN_6$, 3.75%, M^{+2}), 364 ($C_{19}H_{17}ClN_6$, 7.34%, M^+), 76 (C_6H_4, 100%). Anal. calc. for ($C_{19}H_{17}clN_6$) (M.W. = 364): C, 62.55; H, 4.70; N, 23.04%; found: C, 62.73; H, 4.79; N, 22.87%.

4.5. Biological evaluation

4.5.1. *In vitro* cytotoxic activity. Four human tumor cell lines, namely, hepatocellular carcinoma (HePG-2), mammary gland breast cancer (MCF-7), human prostate cancer (PC3), and colorectal carcinoma (HCT-116), were obtained from VACSERA, Cairo, Egypt. Doxorubicin was used as a standard anticancer drug for comparison. The inhibitory effects of our target compounds on cell growth of the above-mentioned cell lines were determined using the MTT assay.[42] Cells were cultured in RPMI-1640 medium with 10% fetal bovine serum. Penicillin (100 μg ml^{-1}) and streptomycin (100 units per ml) antibiotics were added at 37 °C in a 5% CO_2 incubator. The cells were then seeded in a 96-well plate at a density of 1.0 × 10^4 cells per well at 37 °C for 48 h under 5% CO_2. After incubation, the cells were treated with different concentrations of compounds and incubated for 24 h. After 24 h of drug treatment, 20 μl of MTT solution at 5 mg ml^{-1} was added and incubated for 4 h. 100 μl DMSO is added into each well to dissolve the purple formazan formed. A colorimetric assay was performed at a wavelength of 570 nm using

a plate reader (EXL 800, USA). The relative cell viability in percentage was calculated. Individual IC_{50} values of the final target compounds are summarized in Table 1.

4.6. Docking studies

In the present work, all docking experiments were performed for all the final target hybrid structures using Molecular Operating Environment software (MOE2014, https://www.chemcomp.com/Products.htm) to evaluate the free energy of binding and to explore the binding mode toward histone acetyltransferase GCN5. Each experiment used histone acetyltransferase GCN5 retrieved from the Brookhaven Protein Databank (PDB: 5TPX, Resolution: 2.1 Å, https://www.rcsb.org/structure/5TPX) and considered as a target for the docking simulation.[9] Firstly, the crystal structure of the protein was prepared by removing water molecules and retaining the essential chain and the ligand, (1*S*,2*S*)-N^1,N^1-dimethyl-N^2-(3-methyl-[1,2,4]triazolo[3,4-*a*]phthalazin-6-yl)-1-phenylpropane-1,2-diamine (L-45). After that, the protein was protonated, the energy was minimized, and the binding pocket of the protein was defined. The 3D structures of the target compounds were sketched using Chem3D 15.0 and saved in MDL molfile format after minimizing the energy. Molecular docking of the final target compounds was performed using a default protocol against the target receptor. In each case, 20 docked structures were generated using genetic algorithm searches; Affinity dG & London dG were used for scoring 1 and scoring 2, respectively.

Author contributions

A. Ghiaty, A. H. Bayoumi, and H. S. Abulkhair were responsible for the conception and rational design of the work. M. H. El-Shershaby, A. Ghiaty, and H. S. Abulkhair were responsible for the data collection and synthesis of the new compounds. K. El-Adl, H. E. A. Ahmed, and H. S. Abulkhair performed the molecular docking study. A. Ghiaty, A. H. Bayoumi, M. S. El-Zoghbi, and H. S. Abulkhair were responsible for spectral data analysis. M. H. El-Shershaby and M. S. El-Zoghbi conducted the cytotoxicity assay. H E. A. Ahmed and K. El-Adl conducted the *in silico* pharmacokinetic study. All authors discussed the results and contributed to the writing and revision of the original manuscript.

Conflicts of interest

The authors declare that they have no competing financial interests or personal relationships that could have appeared to influence the work reported in this article.

Acknowledgements

The authors would like to express their appreciation to Prof. Dr Magda A. El-Sayed, Professor of Pharmaceutical Chemistry at Horus University in Egypt, for her valuable help throughout proofreading the article and the revision stages.

References

1 J. E. Audia and R. M. Campbell, Histone Modifications and Cancer, *Cold Spring Harb. Perspect. Biol.*, 2016, **8**, a019521, DOI: 10.1101/cshperspect.a019521.
2 J. Qin, B. Wen, Y. Liang, W. Yu and H. Li, Histone Modifications and their Role in Colorectal Cancer (Review), *Pathol. Oncol. Res.*, 2020, **26**, 2023–2033, DOI: 10.1007/s12253-019-00663-8.
3 G. Tallen and K. Riabowol, Keep-ING balance: Tumor suppression by epigenetic regulation, *FEBS Lett.*, 2014, **588**, 2728–2742, DOI: 10.1016/j.febslet.2014.03.011.
4 P. Filippakopoulos and S. Knapp, The bromodomain interaction module, *FEBS Lett.*, 2012, **586**, 2692–2704, DOI: 10.1016/j.febslet.2012.04.045.
5 S. Muller, P. Filippakopoulos and S. Knapp, Bromodomains as therapeutic targets, *Expert Rev. Mol. Med.*, 2011, **13**, e29, DOI: 10.1017/S1462399411001992.
6 A. G. Cochran, A. R. Conery and R. J. Sims, Bromodomains: a new target class for drug development, *Nat. Rev. Drug Discovery*, 2019, **18**, 609–628, DOI: 10.1038/s41573-019-0030-7.
7 M. Brand, A. M. Measures, B. G. Wilson, W. A. Cortopassi, R. Alexander, M. Höss, D. S. Hewings, T. P. C. Rooney, R. S. Paton and S. J. Conway, Small Molecule Inhibitors of Bromodomain–Acetyl-lysine Interactions, *ACS Chem. Biol.*, 2015, **10**, 22–39, DOI: 10.1021/cb500996u.
8 M. Moustakim, P. G. K. Clark, D. A. Hay, D. J. Dixon and P. E. Brennan, Chemical probes and inhibitors of bromodomains outside the BET family, *MedChemComm*, 2016, **7**, 2246–2264, DOI: 10.1039/c6md00373g.
9 M. Moustakim, P. G. K. Clark, L. Trulli, A. L. Fuentes de Arriba, M. T. Ehebauer, A. Chaikuad, E. J. Murphy, J. Mendez-Johnson, D. Daniels, C.-F. D. Hou, Y.-H. Lin, J. R. Walker, R. Hui, H. Yang, L. Dorrell, C. M. Rogers, O. P. Monteiro, O. Fedorov, K. V. M. Huber, S. Knapp, J. Heer, D. J. Dixon and P. E. Brennan, Discovery of a PCAF Bromodomain Chemical Probe, *Angew. Chem.*, 2017, **129**, 845–849, DOI: 10.1002/ange.201610816.
10 T. Liu, X. Wang, W. Hu, Z. Fang, Y. Jin, X. Fang and Q. R. Miao, Epigenetically Down-Regulated Acetyltransferase PCAF Increases the Resistance of Colorectal Cancer to 5-Fluorouracil, *Neoplasia*, 2019, **21**, 557–570, DOI: 10.1016/j.neo.2019.03.011.
11 H. Tuo, X. Zheng, K. Tu, Z. Zhou, Y. Yao and Q. Liu, [Expression of PCAF in hepatocellular carcinoma and its clinical significance], *Xi Bao Yu Fen Zi Mian Yi Xue Za Zhi*, 2013, **29**, 297–300.
12 L. Stimson, M. G. Rowlands, Y. M. Newbatt, N. F. Smith, F. I. Raynaud, P. Rogers, V. Bavetsias, S. Gorsuch, M. Jarman, A. Bannister, T. Kouzarides, E. McDonald, P. Workman and G. W. Aherne, Isothiazolones as inhibitors of PCAF and p300 histone acetyltransferase activity, *Mol. Cancer Ther.*, 2005, **4**, 1521–1532, DOI: 10.1158/1535-7163.MCT-05-0135.
13 G. Hirano, H. Izumi, A. Kidani, Y. Yasuniwa, B. Han, H. Kusaba, K. Akashi, M. Kuwano and K. Kohno, Enhanced Expression of PCAF Endows Apoptosis Resistance in Cisplatin-Resistant Cells, *Mol. Cancer Res.*, 2010, **8**, 864–872, DOI: 10.1158/1541-7786.MCR-09-0458.

14 S. Shagufta and I. Ahmad, An insight into the therapeutic potential of quinazoline derivatives as anticancer agents, *MedChemComm*, 2017, **8**, 871–885, DOI: 10.1039/C7MD00097A.

15 M. S. Alesawy, A. A. Al-Karmalawy, E. B. Elkaeed, M. Alswah, A. Belal, M. S. Taghour and I. H. Eissa, Design and discovery of new 1,2,4-triazolo[4,3-*c*]quinazolines as potential DNA intercalators and topoisomerase II inhibitors, *Arch. Pharm.*, 2020, DOI: 10.1002/ardp.202000237.

16 M. H. Hannoun, M. Hagras, A. Kotb, A.-A. M. M. El-Attar and H. S. Abulkhair, Synthesis and antibacterial evaluation of a novel library of 2-(thiazol-5-yl)-1,3,4-oxadiazole derivatives against methicillin-resistant *Staphylococcus aureus* (MRSA), *Bioorg. Chem.*, 2020, **94**, 103364, DOI: 10.1016/J.BIOORG.2019.103364.

17 H. A. Mahdy, M. K. Ibrahim, A. M. Metwaly, A. Belal, A. B. M. Mehany, K. M. A. El-Gamal, A. El-Sharkawy, M. A. Elhendawy, M. M. Radwan, M. A. Elsohly and I. H. Eissa, Design, synthesis, molecular modeling, in vivo studies and anticancer evaluation of quinazolin-4(3H)-one derivatives as potential VEGFR-2 inhibitors and apoptosis inducers, *Bioorg. Chem.*, 2020, **94**, 103422, DOI: 10.1016/j.bioorg.2019.103422.

18 A. Turky, A. H. Bayoumi, A. Ghiaty, A. S. El-Azab, A. A.-M. Abdel-Aziz and H. S. Abulkhair, Design, synthesis, and antitumor activity of novel compounds based on 1,2,4-triazolophthalazine scaffold: Apoptosis-inductive and PCAF-inhibitory effects, *Bioorg. Chem.*, 2020, 104019, DOI: 10.1016/j.bioorg.2020.104019.

19 H. G. Ezzat, A. H. Bayoumi, F. F. Sherbiny, A. M. El-Morsy, A. Ghiaty, M. Alswah and H. S. Abulkhair, Design, synthesis, and molecular docking studies of new [1,2,4]triazolo[4,3-a]quinoxaline derivatives as potential A2B receptor antagonists, *Mol. Divers.*, 2021, **25**, 291–306, DOI: 10.1007/s11030-020-10070-w.

20 A. Turky, A. H. Bayoumi, F. F. Sherbiny, K. El-Adl and H. S. Abulkhair, Unravelling the anticancer potency of 1,2,4-triazole-N-arylamide hybrids through inhibition of STAT3: synthesis and in silico mechanistic studies, *Mol. Divers.*, 2021, **25**, 403–420, DOI: 10.1007/s11030-020-10131-0.

21 S. I. Kovalenko, Synthesis and Anticancer Activity of 2-(Alkyl-, Alkaryl-, Aryl-, Hetaryl-)[1,2,4]triazolo[1,5-c]quinazolines, *Sci. Pharm.*, 2013, **81**, 359–391, DOI: 10.3797/scipharm.1211-08.

22 O. M. Antypenko, S. I. Kovalenko, O. V. Karpenko, V. O. Nikitin and L. M. Antypenko, Synthesis, Anticancer, and QSAR Studies of 2-Alkyl(aryl,hetaryl)quinazolin-4(3 H)-thione's and [1,2,4]Triazolo-[1,5- c]quinazoline-2-thione's Thioderivatives, *Helv. Chim. Acta*, 2016, **99**, 621–631, DOI: 10.1002/hlca.201600062.

23 M. Driowya, J. Leclercq, V. Verones, A. Barczyk, M. Lecoeur, N. Renault, N. Flouquet, A. Ghinet, P. Berthelot and N. Lebegue, Synthesis of triazoloquinazolinone based compounds as tubulin polymerization inhibitors and vascular disrupting agents, Eur, *J. Med. Chem.*, 2016, **115**, 393–405, DOI: 10.1016/j.ejmech.2016.03.056.

24 R. Al-Salahi, M. Marzouk, A. E. Ashour and I. Alswaidan, Synthesis and Antitumor Activity of 1,2,4-Triazolo[1,5-a]-quinazolines, *Asian J. Chem.*, 2014, **26**, 2173–2176, DOI: 10.14233/ajchem.2014.16849.

25 W. A. Ewes, M. A. Elmorsy, S. M. El-Messery and M. N. A. Nasr, Synthesis, biological evaluation and molecular modeling study of [1,2,4]-Triazolo[4,3-c]quinazolines: New class of EGFR-TK inhibitors, *Bioorg. Med. Chem.*, 2020, **28**, 115373, DOI: 10.1016/j.bmc.2020.115373.

26 M. S. Alesawy, A. A. Al-Karmalawy, E. B. Elkaeed, M. Alswah, A. Belal, M. S. Taghour and I. H. Eissa, Design and discovery of new 1,2,4-triazolo[4,3-*c*]quinazolines as potential DNA intercalators and topoisomerase II inhibitors, *Arch. Pharm.*, 2020, **354**, 2000237, DOI: 10.1002/ardp.202000237.

27 H. S. Abulkhair, A. Turky, A. Ghiaty, H. E. A. Ahmed and A. H. Bayoumi, Novel triazolophthalazine-hydrazone hybrids as potential PCAF inhibitors: Design, synthesis, in vitro anticancer evaluation, apoptosis, and molecular docking studies, *Bioorg. Chem.*, 2020, **100**, 103899, DOI: 10.1016/j.bioorg.2020.103899.

28 Y. C. Martin, A practitioner's perspective of the role of quantitative structure-activity analysis in medicinal chemistry, *J. Med. Chem.*, 1981, **24**, 229–237, DOI: 10.1021/jm00135a001.

29 G. A. Patani and E. J. LaVoie, Bioisosterism: A Rational Approach in Drug Design, *Chem. Rev.*, 1996, **96**, 3147–3176, DOI: 10.1021/cr950066q.

30 L. Lima and E. Barreiro, Bioisosterism: A Useful Strategy for Molecular Modification and Drug Design, *Curr. Med. Chem.*, 2005, **12**, 23–49, DOI: 10.2174/0929867053363540.

31 G. Papadatos and N. Brown, *In silico* applications of bioisosterism in contemporary medicinal chemistry practice, *Wiley Interdiscip. Rev.: Comput. Mol. Sci.*, 2013, **3**, 339–354, DOI: 10.1002/wcms.1148.

32 K. El-Adl, M. K. Ibrahim, F. Khedr, H. S. Abulkhair and I. H. Eissa, N-Substituted-4-phenylphthalazin-1-amine derived VEGFR-2 inhibitors: Design, synthesis, molecular docking and anticancer evaluation studies, *Arch. Pharm.*, 2020, e202000219, DOI: 10.1002/ardp.202000219.

33 A. Turky, F. F. Sherbiny, A. H. Bayoumi, H. E. A. Ahmed and H. S. Abulkhair, Novel 1,2,4-triazole derivatives: Design, synthesis, anticancer evaluation, molecular docking, and pharmacokinetic profiling studies, *Arch. Pharm.*, 2020, **353**, 2000170, DOI: 10.1002/ardp.202000170.

34 K. El-Adl, H. Sakr, S. S. A. El-Hddad, A. A. El-Helby, M. Nasser and H. S. Abulkhair, Design, synthesis, docking, ADMET profile, and anticancer evaluations of novel thiazolidine-2,4-dione derivatives as VEGFR-2 inhibitors, *Arch. Pharm.*, 2021, 2000491, DOI: 10.1002/ardp.202000491.

35 A. A. El-Helby, H. Sakr, I. H. Eissa, H. Abulkhair, A. A. Al-Karmalawy and K. El-Adl, Design, synthesis, molecular docking, and anticancer activity of benzoxazole derivatives as VEGFR-2 inhibitors, *Arch. Pharm.*, 2019, **352**, 1900113, DOI: 10.1002/ardp.201900113.

36 H. Abul-Khair, S. Elmeligie, A. Bayoumi, A. Ghiaty, A. El-Morsy and M. H. Hassan, Synthesis and Evaluation of Some New (1,2,4) Triazolo(4,3-*a*)Quinoxalin-4(5*H*)-one Derivatives as AMPA Receptor Antagonists, *J. Heterocycl. Chem.*, 2013, **50**, 1202–1208, DOI: 10.1002/jhet.714.

37 H. S. Abulkhair, S. Elmeligie, A. Ghiaty, A. El-Morsy, A. H. Bayoumi, H. E. A. Ahmed, K. El-Adl, M. F. Zayed, M. H. Hassan, E. N. Akl and M. S. El-Zoghbi, *In vivo*- and *in silico*-driven

identification of novel synthetic quinoxalines as anticonvulsants and AMPA inhibitors, *Arch. Pharm.*, 2021, **354**, 2000449, DOI: 10.1002/ardp.202000449.

38 S. K. Babu, V. Prabhakar, L. K. Ravindranath, S. S. Prasad and J. Latha, Synthesis, characterization and biological evaluation of some novel quinazoline derivatives as potential antimicrobial agents, *J. Chem. Chem. Sci.*, 2016, **6**, 648–664.

39 A. M. El-Morsy, M. S. El-Sayed and H. S. Abulkhair, Synthesis, Characterization and *In Vitro* Antitumor Evaluation of New Pyrazolo[3,4-*d*]Pyrimidine Derivatives, *Open J. Med. Chem.*, 2017, **07**, 1–17, DOI: 10.4236/ojmc.2017.71001.

40 A. M. Omar, S. Ihmaid, E.-S. S. E. Habib, S. S. Althagfan, S. Ahmed, H. S. Abulkhair, H. E. A. Ahmed and H. E. A. Ahmed, The Rational Design, Synthesis, and Antimicrobial Investigation of 2-Amino-4-Methylthiazole Analogues Inhibitors of GlcN-6-P Synthase, *Bioorg. Chem.*, 2020, **99**, 103781, DOI: 10.1016/j.bioorg.2020.103781.

41 A. A. El-Helby, R. R. A. Ayyad, M. F. Zayed, H. S. Abulkhair, H. Elkady and K. El-Adl, Design, synthesis, in silico ADMET profile and GABA-A docking of novel phthalazines as potent anticonvulsants, *Arch. Pharm.*, 2019, **352**, 1800387, DOI: 10.1002/ardp.201800387.

42 T. Mosmann, Rapid colorimetric assay for cellular growth and survival: application to proliferation and cytotoxicity assays, *J. Immunol. Methods*, 1983, **65**, 55–63.

43 M. Le Grazie, M. R. Biagini, M. Tarocchi, S. Polvani and A. Galli, Chemotherapy for hepatocellular carcinoma: The present and the future, *World J. Hepatol.*, 2017, **9**, 907, DOI: 10.4254/wjh.v9.i21.907.

44 K. W. Wellington, Understanding cancer and the anticancer activities of naphthoquinones – a review, *RSC Adv.*, 2015, **5**, 20309–20338, DOI: 10.1039/C4RA13547D.

45 I. Kufareva and R. Abagyan, *Methods of Protein Structure Comparison*, Springer, 2011, pp. 231–257, DOI: 10.1007/978-1-61779-588-6_10.

46 C. A. Lipinski, F. Lombardo, B. W. Dominy and P. J. Feeney, Experimental and computational approaches to estimate solubility and permeability in drug discovery and development settings, *Adv. Drug Delivery Rev.*, 1997, **23**, 3–25, DOI: 10.1016/S0169-409X(96)00423-1.

47 D. F. Veber, S. R. Johnson, H.-Y. Cheng, B. R. Smith, K. W. Ward and K. D. Kopple, Molecular Properties That Influence the Oral Bioavailability of Drug Candidates, *J. Med. Chem.*, 2002, **45**, 2615–2623, DOI: 10.1021/jm020017n.

48 D. E. V. Pires, T. L. Blundell and D. B. Ascher, pkCSM: Predicting Small-Molecule Pharmacokinetic and Toxicity Properties Using Graph-Based Signatures, *J. Med. Chem.*, 2015, **58**, 4066–4072, DOI: 10.1021/acs.jmedchem.5b00104.

49 A. Beig, R. Agbaria and A. Dahan, Oral Delivery of Lipophilic Drugs: The Tradeoff between Solubility Increase and Permeability Decrease When Using Cyclodextrin-Based Formulations, *PLoS One*, 2013, **8**, e68237, DOI: 10.1371/journal.pone.0068237.

50 A. Hebert, M. Bishop, D. Bhattacharyya, K. Gleason and S. Torosian, Assessment by Ames test and comet assay of toxicity potential of polymer used to develop field-capable rapid-detection device to analyze environmental samples, *Appl. Nanosci.*, 2015, **5**, 763–769, DOI: 10.1007/s13204-014-0373-7.

51 S. Roy and M. K. Mathew, Fluid flow modulates electrical activity in cardiac hERG potassium channels, *J. Biol. Chem.*, 2018, **293**, 4289–4303, DOI: 10.1074/jbc.RA117.000432.

52 X. Wu, Q. Zhang and J. Hu, QSAR study of the acute toxicity to fathead minnow based on a large dataset, *SAR QSAR Environ. Res.*, 2016, **27**, 147–164, DOI: 10.1080/1062936X.2015.1137353.

